



CIVIL ENGINEERING STUDIES  
Illinois Center for Transportation Series No. 12-023  
UILU-ENG-2012-2026  
ISSN: 0197-9191

# FATIGUE PERFORMANCE OF BRASS BREAKAWAY LIGHT POLE COUPLINGS

Prepared By  
**Joseph Rudd**  
**Gregory Banas**  
University of Illinois at Urbana-Champaign  
**Christopher Hahin**  
Illinois Department of Transportation

Research Report FHWA-ICT-12-023

A report of the findings of  
ICT-R27-80  
**Fatigue of Brass Breakaway Couplings**

Illinois Center for Transportation

April 2013

**Technical Report Documentation Page**

1. Report No. FHWA-ICT-2012-023		2. Government Accession No.		3. Recipient's Catalog No.	
4. Title and Subtitle Fatigue Performance of Brass Breakaway Light Pole Couplings				5. Report Date April 2013	
				6. Performing Organization Code	
7. Author(s) Joseph Rudd and Gregory Banas of the University of Illinois Christopher Hahin of the Illinois Department of Transportation				8. Performing Organization Report No. ICT-2012-023 UILU-ENG-2012-2026	
9. Performing Organization Name and Address Illinois Center for Transportation Department of Civil and Environmental Engineering University of Illinois at Urbana-Champaign 205 N. Mathews, MC 250 Urbana, IL 61801				10. Work Unit No. (TRAIS)	
				11. Contract or Grant No. R27-80	
12. Sponsoring Agency Name and Address Illinois Department of Transportation Bureau of Materials and Physical Research 126 East Ash St. Springfield, IL 62704				13. Type of Report and Period Covered	
				14. Sponsoring Agency Code	
15. Supplementary Notes This project was completed through the joint efforts of the University of Illinois at Urbana-Champaign and the Illinois Department of Transportation on behalf of the State of Illinois and the Federal Highway Administration.					
16. Abstract Breakaway couplings connect light pole bases to foundation anchor bolts and are intended to fracture on impact after vehicle collision to protect drivers and passengers from severe injury. The coupling consists of an internally threaded hollow hexagon made of half-hard CDA 360 brass with a thread-locked stainless steel stud. Several designs of the notched hexagonal shaped coupling were tested in bending by attaching them to a simulated pole tube and base and then inducing stresses by deflection of the tube by a hydraulic jack. Individual couplings were also fatigued in axial tension-compression by a servo-controlled universal testing machine. Using the data obtained, the axial tension-compression fatigue relationship for the brass couplings was $\Delta S = 433 N^{-0.153}$ , where $\Delta S$ is the alternating stress from tension to compression. Finite element analysis using ABAQUS® found that stress concentrations in the external notch radius and the internal threads were accurate to about 20% of the values obtained from experimental strain gage data.  The stress concentration factors for the final design were determined to be $K_{tt} = 10.8$ in tension and $K_{tc} = 10.4$ in compression. Couplings were fatigue tested in laboratory air at room temperatures in the range of $10^4$ to $10^7$ cycles. Couplings that were exposed to 1000 hr of salt fog prior to fatigue testing showed no difference in fatigue life compared to couplings fatigued in air.  Standard structural theory was used to determine the nominal stresses of couplings attached to steel poles subjected to winds of 90 mph. Using an average stress concentration factor $K_{t,avg}$ of 10.6, the peak coupling stress in various orientations of the pole base with respect to the wind direction was determined to be 24.1 ksi. When a more accurate segmental wind pressure method of determining moments acting on the pole base was used, the calculated peak stress was 23.9 ksi. At 90 mph, a +24 ksi to -24 ksi alternating stress develops, resulting in a 50% mean fatigue life estimated at 1,799,000 cycles.  Variances in notch section were caused by straightness deviations of hexagon stock and from drilling and tapping operations, averaging 4.2% to a maximum of 9%. The fatigue initiation zone was about 30° of the notch circumference. The probability that four couplings would have only the weakest one facing the maximum wind exposure is $30^0/360^0/4$ , which is about 2% of the time. Maximum wind speeds recorded in Illinois are less than the 90 mph AASHTO requirement. Decreasing notch depth by 9% would lessen the likelihood of premature failure due to insufficient load-bearing section of the coupling notch.					
17. Key Words Breakaway couplings; CDA 360 brass; fatigue life; stress concentration factor; light poles; wind pressures; finite element methods			18. Distribution Statement No restrictions. This document is available to the public through the National Technical Information Service, Springfield, Virginia 22161		
19. Security Classification (of this report) Unclassified		20. Security Classification (of this page) Unclassified		21. No. of Pages 50 pp. plus appendix	
				22. Price	

## **ACKNOWLEDGMENTS AND DISCLAIMER**

This publication is based on the results of ICT-R27-80, Fatigue Testing of Breakaway Couplings. ICT-R27-80 was conducted in cooperation with the Illinois Center for Transportation; the Illinois Department of Transportation (IL DOT); and the U.S. Department of Transportation, Federal Highway Administration (FHWA).

Members of the Technical Review Panel are the following:

Mr. Christopher Hahin, IL DOT Bureau of Materials & Physical Research, TRP Chair

Mrs. Patricia Broers, IL DOT Bureau of Materials & Physical Research

Mr. Tim Kell, IL DOT Bureau of Construction

Mr. Mark Seppelt, IL DOT Bureau of Design and Environment

Mr. Brian Pfeiffer, FHWA

Mr. David Piper, IL DOT Bureau of Safety Engineering

This project was jointly completed by the University of Illinois and the Illinois Department of Transportation (IL DOT). Mr. Joseph Rudd of the University of Illinois, who wrote the majority of this report, acknowledges the support of his mentor, Dr. Gregory Banas, for many revisions of this report and laboratory support; also acknowledges Mr. Christopher Hahin of IL DOT, the inventor of the brass breakaway coupling, for his inputs on the fatigue of brass and light poles; Dr. Hussam Mahmoud of the University of Illinois, for his assistance on the use of finite element modeling; and other University of Illinois faculty members, including Prof. Leslie Struble, who provided important advice concerning this work and Prof. Fred Lawrence and Prof. Darrell Socie for their intellectual input.

Mr. Hahin acknowledges the machining of various brass coupling designs and helpful advice of Mr. Perry Walter and Mr. Chris Murphy, as well as the impact testing of brass and tensile testing of couplings conducted by Mr. Terry Havard and Mr. Steve Blickhan of the Bureau of Materials & Physical Research. The 1000 hr salt spray exposure of couplings by Ms. Susan Drodz of the U.S. Army Construction Engineering Research Lab is acknowledged. The advice of Dr. Ronald Faller of the University of Nebraska and Dr. Roger Bligh of the Texas Transportation Institute on pendulum impact testing is also acknowledged.

The contents of this report reflect the view of the authors, who are responsible for the facts and the accuracy of the data presented herein. The contents do not necessarily reflect the official views or policies of the Illinois Center for Transportation, the Illinois Department of Transportation, or the Federal Highway Administration. This report does not constitute a standard, specification, or regulation.

Trademark or manufacturers' names appear in this report only because they are considered essential to the object of this document and do not constitute an endorsement of product by the Federal Highway Administration, the Illinois Department of Transportation, or the Illinois Center for Transportation.

## EXECUTIVE SUMMARY

Breakaway couplings connect light pole bases to several anchor bolts in concrete foundations. They are used to prevent injury to drivers and passengers in case of vehicular collision with light poles. Bending and axial tension-compression tests were performed at the University of Illinois on several coupling designs and specimens provided by the Illinois Department of Transportation. Couplings were made of half-hard Copper Development Association (CDA) 360 free-cutting brass with internal threading and an external notch cut to a depth of 0.150 in. for the first design. Couplings attached to light pole bases were tested in square, diamond, and individual loading configurations. The stress concentration factor,  $K_{tb}$ , of the notched section of hexagons of the first design was determined to be 5.70 by strain measurements. This value is slightly higher than the theoretical stress concentration factor of 4.7. Fatigue tests were also performed on the notched specimens of the first design in full compression-tension reversal using force control. An elastic tension-compression test was performed to determine both tensile and compressive stress concentration factors. In tension,  $K_{tt} = 7.26$ , while in compression  $K_{tc} = 6.80$ .

Bending testing was performed on a second design using only a single coupling in which the depth of the notch was increased to 0.155 in., the external notch radius was decreased to 1/16 in., and the bevel was removed. The stress concentration factor,  $K_{tb}$ , was determined to be 9.0 by use of an extensometer across the notch and a strain gage on the nominal section. Fatigue tests were also performed on notched specimens made of CDA 360 brass of the second design in full compression-tension reversal using force control. An elastic tension-compression test was performed to determine both tensile and compressive stress concentration factors. In tension,  $K_{tt} = 10.80$ , and in compression  $K_{tc} = 10.40$ .

Fatigue testing was performed in the long-life regime ( $10^4$ - $10^7$  cycles) on both coupling geometries. Because of minor eccentricities in both the coupling and testing set-up, higher bending stresses were recorded during testing, which most likely contributed to the variability in fatigue life measurements.

Finite element modeling of a two-dimensional cross-section of the coupling was performed using ABAQUS®. A reduced cross-section was used to successfully run the model and good agreement between modeling and experimental data was achieved for the complex geometry.

Using wind pressures for tapered 40 ft cylindrical steel light poles sustaining 90 mph winds, the peak stresses in the brass couplings were calculated by standard structural theory. The AASHTO method was used to calculate nominal stresses. The peak tensile stress was determined to be about 24.1 ksi, taking stress concentrations into account. When a more detailed segmental method, taking more precise determinations of drag and height coefficients into account was used and applying a  $K_{tavg}$  of 10.6, the peak stress was calculated to be 23.9 ksi. At the 90 mph stress level of 23.9 ksi ( $\Delta S = 47.8$ ), the 50% mean fatigue life was calculated to be 1,799,000 cycles. This fatigue life was based on the fatigue relationship developed in this study,  $\Delta S = 433 N^{-0.153}$ , which was derived from axial tension-compression testing of individual couplings.

When variations in threads or wall thickness in the notched zone were considered, peak tensile stresses were calculated at 90 mph winds to rise to  $23.9 \times 1.39 = 33.2$  ksi. A 40 ft aluminum pole with a wall thickness of 0.250 in. weighs about 210 lb and a 7 gage wall steel pole about 265 lb. The weight of a steel pole decreases tensile stress by  $-2.3$  ksi because of compression of the couplings, taking a stress concentration factor 10.4 into account. This further reduces tensile stresses to  $(33.2 \text{ ksi} - 2.3 \text{ ksi}) = 30.9$  ksi, resulting in cyclic reversal of  $+30.9$  ksi in tension to  $-35.5$  ksi in compression and a mean stress of  $-2.3$  ksi. Compressive mean stresses improve fatigue life by permitting an increase of the alternating stress compared to its value at a mean stress of zero.

Neglecting the contribution of compressive mean stress, a light pole at 90 mph wind speed with a peak tensile stress of 33.2 ksi and a stress range of 68.7 ksi would have a fatigue life of 166,810 cycles. For a 90 mph wind storm of 30 minutes duration, which is beyond the limits of weather data recorded in Illinois, couplings would sustain 1800 stress cycles. Because steel light poles typically have fundamental frequencies near 1 Hz, this would consume about 1.1% of available fatigue life. Aluminum light poles have higher fundamental frequencies near 3 Hz, consuming about 3.3% of their available fatigue life.

Although the specimens exhibited variations from drilling, tapping and cutting of notches, the use of single specimens in fatigue testing gives the impression of a limited fatigue life in actual service. However, this impression can be misleading because there are other factors that extend life in actual service. Although wall thickness of the notch varied on average of 4.2% up to 9.1% maximum, the probability that all couplings will have their weakest orientation perfectly aligned for premature failure is small. Since  $30^\circ$  of the thread notch circumference is the susceptible fatigue zone, the probability of alignment with a high-speed wind direction is about  $30^\circ/360^\circ$ . The probability that all four couplings will be perfectly aligned will be even smaller at  $30^\circ/360^\circ/4 = 0.021$ , which is 2.1% of the time. A 9% increase in notch wall thickness should take variations into account that are derived from hexagon straightness tolerances and any slight deviations from chucking, drilling, and tapping operations.

# CONTENTS

<b>LIST OF FIGURES .....</b>	<b>vi</b>
<b>LIST OF TABLES .....</b>	<b>viii</b>
<b>CHAPTER 1 INTRODUCTION .....</b>	<b>1</b>
<b>CHAPTER 2 LITERATURE REVIEW .....</b>	<b>3</b>
<b>CHAPTER 3 EXPERIMENTAL PROCEDURES .....</b>	<b>5</b>
<b>3.1 Specimens.....</b>	<b>5</b>
3.1.1 Bending Tests of Design 1 .....	5
3.1.2 Monotonic Tests.....	5
3.1.3 Fatigue Tests of Design 1 .....	6
3.1.4 Bending Tests of Design 2.....	7
3.1.5 Fatigue Tests of Design 2.....	7
3.1.6 Fatigue Testing of Design 2 with Salt Spray .....	7
<b>3.2 Testing Setup.....</b>	<b>7</b>
3.2.1 Bending Tests of Design 1 .....	7
3.2.2 Monotonic Tests.....	10
3.2.3 Fatigue Tests of Design 1 .....	10
3.2.4 Bending Tests of Design .....	10
3.2.5 Fatigue Tests of Design 2 .....	10
3.2.6 Fatigue Tests of Design 2 with Salt Spray .....	10
<b>3.3 Testing Process.....</b>	<b>11</b>
3.3.1 Bending Tests of Design 1 .....	11
3.3.2 Monotonic Tests.....	11
3.3.3 Fatigue Tests of Design 1 .....	11
3.3.4 Bending Tests of Design 2.....	12
3.3.5 Fatigue Tests Design 2 .....	12
3.3.6 Fatigue Tests of Design 2 with Salt Spray .....	12
<b>CHAPTER 4 RESULTS AND DISCUSSION.....</b>	<b>13</b>
<b>4.1 Bending Tests Design 1 .....</b>	<b>13</b>
<b>4.2 Monotonic Tests .....</b>	<b>16</b>
<b>4.3 Fatigue Tests Design 1 .....</b>	<b>18</b>
<b>4.4 Bending Tests for Design 2.....</b>	<b>23</b>
<b>4.5 Fatigue Tests for Design 2.....</b>	<b>23</b>

4.6 Fatigue Tests Design 2 with Salt Spray.....	24
4.7 Fracture Surface Analysis .....	26
CHAPTER 5 FINITE ELEMENT ANALYSIS .....	35
CHAPTER 6 EFFECTS OF WIND LOADS ON COUPLINGS .....	38
CHAPTER 7 BENDING STRESSES AND FATIGUE LIFE.....	43
CHAPTER 8 CONCLUSIONS .....	46
CHAPTER 9 FURTHER STUDY .....	48
REFERENCES.....	49
APPENDIX.....	A-1

## LIST OF FIGURES

Figure 1. Coupling design 1. ....	1
Figure 2. Coupling design 2. ....	2
Figure 3. Strain gage placement. ....	5
Figure 4. Tensile specimen geometry (in.).....	6
Figure 5. Loading plate design.....	8
Figure 6. Concrete block before chipping. ....	8
Figure 7. Concrete block after chipping. ....	9
Figure 9. Diamond loading configuration. ....	10
Figure 10. Fatigue grips (dimensions in inches). ....	11
Figure 11. Theoretical vs. recorded strain in diamond configuration. ....	13
Figure 12. Theoretical vs. recorded strain in square configuration. ....	14
Figure 13. Theoretical vs. recorded strain loading of coupling 1.....	14
Figure 14. Theoretical vs. recorded strain loading of coupling 2.....	15
Figure 15. Eccentricity of couplings resulting from testing setup, in inches. ....	16
Figure 16. CDA 360 0.500 in. round tensile specimen 1.....	17
Figure 17. CDA 360 0.500 in. round tensile specimen 2.....	17
Figure 18. CDA 360 0.500 in. round tensile specimen 3.....	18
Figure 19. S-N curve of notched brass couplings (without bending stresses). ....	20
Figure 20. S-N curve of notched brass couplings (with bending stresses). ....	20
Figure 21. Coupling eccentricity measurement.....	21
Figure 22. Comparison of uniaxial and rotating-bending fatigue of polymer.....	22
Figure 23. Comparison of uniaxial and rotating-bending fatigue of CDA 365. ....	23
Figure 24. S-N curve of notched brass couplings (with bending stresses). ....	25
Figure 25. Fracture surface of coupling 6. ....	26
Figure 26. Fracture surface of coupling 7. ....	27
Figure 27. Fracture surface of coupling 8. ....	27
Figure 28. Fracture surface of coupling 9. ....	28
Figure 29. Fracture surface of coupling 10. ....	28
Figure 30. Fracture surface of coupling 0. ....	29
Figure 31. Fracture surface of coupling 31. ....	29
Figure 32. Fracture surface of coupling 41. ....	30
Figure 33. Fracture surface of coupling 42. ....	30
Figure 34. Fracture surface of coupling 43. ....	31
Figure 35. Fracture surface of coupling 44. ....	31
Figure 36. Fracture surface of coupling 45. ....	32
Figure 37. Fracture surface of coupling 46. ....	32
Figure 38. Fracture surface of coupling 51 (failed in tension). ....	33
Figure 39. Fracture surface of coupling 52. ....	33
Figure 40. Fracture surface of coupling 53. ....	34
Figure 41. Fracture surface of coupling 54. ....	34
Figure 42. Two-dimensional cross section.....	35
Figure 43. Minimal section analyzed with loading conditions.....	36

Figure 44. Representative element density of the finite element model. ....	36
Figure 45. Finite element stress ranges of critical notches. ....	37
Figure 46. Drag coefficients at various pole heights and respective diameters for a 40 ft tapered pole with a 10 in. base and 4 in. at the top, at a 90 mph wind speed. ....	39
Figure 47. Height coefficients for a light pole at 5 ft intervals, based on the equation $C_h = [Z / 33]^{0.28}$ . ....	40

## LIST OF TABLES

Table 1. Chemical Composition for CDA 360 .....	6
Table 2. Nominal Strain at Notch Strain of $724 \mu\epsilon$ .....	15
Table 3. Material Properties of CDA 360 .....	18
Table 4. Fatigue Results for Design 1 (Without Bending Stresses) .....	19
Table 5. Stress Concentration Factors for Design 1 .....	19
Table 6. Eccentricity in Couplings (in.) .....	22
Table 7. Bending Stresses Under Fatigue for Design 2 .....	24
Table 8. Fatigue Results for Design 2 (Without Bending Stresses) .....	24
Table 9. Fatigue Performance of Couplings Suggested to Salt Spray .....	25
Table 10. Summary of Drag and Height Coefficients, Diameters, Forces and Moments .....	41
Table 11. Summary of Peak Concentrated Stresses at Various Wind Speeds .....	42

## CHAPTER 1 INTRODUCTION

Alloy steels and aluminum die castings have typically been used for couplings that connect light pole bases to foundation anchor bolts, breaking away upon pole impact by a vehicle. The current replacement breakaway coupling used in Illinois is manufactured by Transpo Industries, which has a double-hourglass configuration and is made of ETD 150 high strength steel (Transpo Industries, no date). To reduce the cost of replacing couplings that have failed or are at the end of their useful life, CDA 360 brass was chosen as a potential alternative material because of its uniform, higher fracture toughness over normal operating temperatures and its fatigue characteristics.

The first series of designs were determined and refined using drop weight impact tests. The first notch design tested in this study is depicted in Figure 1 (Design 1). The following designs were refined from results from pendulum impact testing conducted at the University of Nebraska, whereby the bevel was removed; the depth of the notch increased to 0.155 in., and the notch radius was sharpened from 1/8 in. to 1/16 in. The second design removed the bevel, decreased the notch radius to 1/16 in., and the depth of the notch was increased by 0.005 in., as shown in Figure 2 (Design 2).

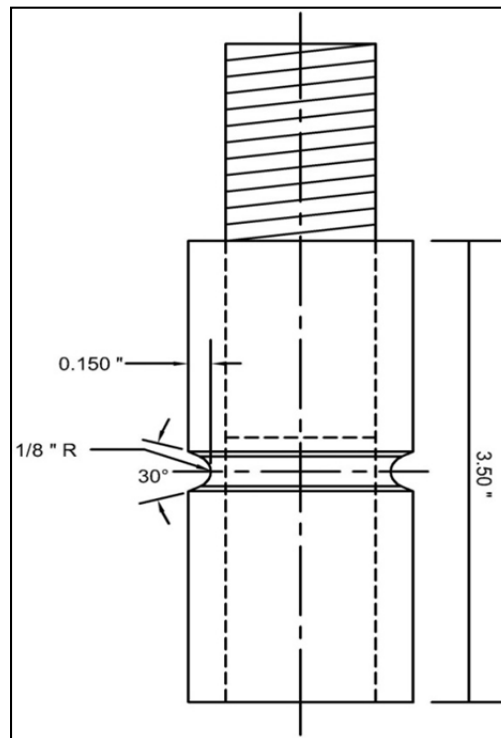


Figure 1. Coupling design 1.

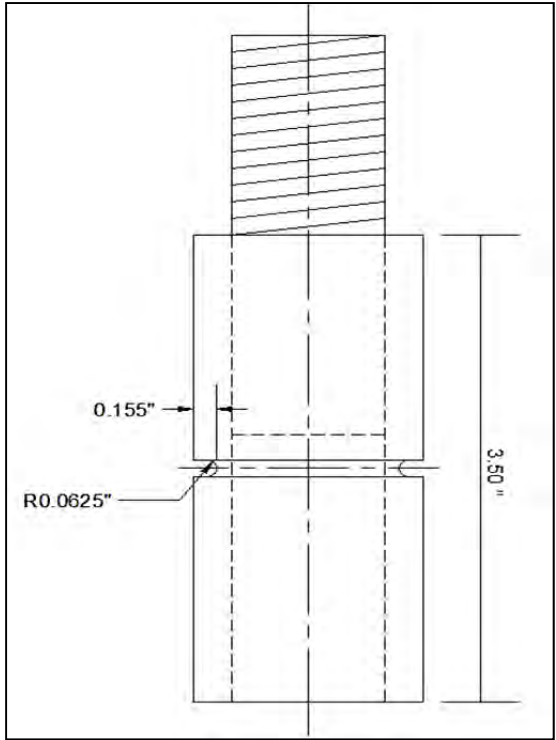


Figure 2. Coupling design 2.

## CHAPTER 2 LITERATURE REVIEW

Design and testing of breakaway hardware for light poles began in the 1950s in England, with significant research performed by Stoughten et al. (1989), Elmarakbi et al. (2006), Walton et al. (1973), and Zegeer and Cynecki (1986).

Stoughten et al. (1989) researched aluminum breakaway couplings and slip bases with a variety of light poles by impacting the assemblies with a 1979 Honda Civic. The aluminum breakaway couplings showed a maximum change in velocity of 12.4 ft/sec, which was within the limits of the 1985 AASHTO specifications, but were not recommended for use because of a high level of porosity in the fracture surfaces and lack of compliance with tension or shear tests specified by the California Department of Transportation. The slip bases in the study performed adequately.

Zegeer and Cynecki (1986), in association with the Federal Highway Administration (FHWA), created a user's manual for evaluating the economic effects of addressing utility pole accidents and provided a number of recommendations to reduce the number of collisions with poles, using examples from a thorough literature review. Walton et al. (1973) conducted further crash tests of light poles using frangible bases, determining that those bases performed acceptably and would not pose any significant hazard by obstructing traffic.

Elmarakbi et al. (2006) investigated finite element modeling of the impact of various types of light poles with varying support systems, including bolted connections, poles embedded in soil, and poles embedded in sand. They determined that embedded poles absorbed significantly more energy than poles attached to concrete bases, but concluded that embedded poles were preferential because the poles did not fall over.

Transpo double-hourglass-shaped couplings received FHWA approval for use March 1996 and January 1997, according to FHWA Letters of Acceptance LS045. Fatigue life was not a part of this acceptance. Research performed by Azzam and Menzemer (2006a, 2006b) on the residual stresses from the welding of supports for aluminum light poles, which included finite element modeling and fatigue behavior, showed that high residual stresses were present from the welding process. By changing the plate thickness from 1 to 2 in., residual stresses decreased by 24%, and the constant amplitude fatigue life (CAFL) was increased.

The fatigue strength for half-hard CDA 360 free-cutting brass, based on rotating bending of smooth, 9 mm diameter specimens taken from 50 mm diameter rounds, is 20 ksi at  $10^8$  cycles and 14 ksi at  $3 \times 10^8$  cycles (Tyler 1990). No low-cycle fatigue data were available for CDA 360 brass used for the couplings in this study, but some fatigue data for other brass alloys of similar composition were available.

Moore and Lewis (1931) analyzed pure copper, a brass alloy, and an aluminum alloy in fatigue by applying shear stresses. McAdam (1925) investigated the effect of cold work on metals on their fatigue lives. Because the couplings are made of half-hard CDA 360 and machined after being formed, the residual stresses from cold working can be as high as the yield stress of the material if not stress relieved (McAdam 1925). Because monotonic tests were performed, the ability to predict the fatigue life using the stress vs. strain curve was considered. Using information presented by Ong (1993) and combined with estimates from Moore and Lewis's (1931) research, a combined method of prediction was developed, in which observed fatigue life was similar to predicted expectations.

Akyildiz and Livatyali (2010) performed research on the effects of external threading on fatigue behavior, determining that machining parameters have a complex relationship with fatigue life. Cutting tool sharpness showed the largest effect, followed by cutting velocity. Fatigue cracks initiated at the roots of the external threads.

Berger et al. (2006) studied the effect of notches on fatigue life of aluminum alloys, showing that notched specimens always displayed cracks initiating from the surface, while non-notched specimens could show crack initiations from internal defects, even for specimens with notches of relatively low stress concentrations ( $K_t = 1.8$ ).

Mnif et al. (2010) studied pre-strain and over-strain for their effects on fatigue behavior of brass alloys, showing that pre-strain may cause strain hardening and slip band formation, which were often the points of crack initiation, which reduced fatigue life.

Finite element analysis of threaded specimens has been a limited area of thorough study because of the complex geometry of threads. Tanaka et al. (1981) performed some of the earliest work on modeling realistic threads using finite element analysis software, reaffirming that the distribution of stresses across engaged threads is definitely non-uniform, with the first threads carrying significantly more load than following threads. Fukuoka and Takaki (2003) showed that finite element modeling could sufficiently simulate stresses induced during tightening, even after yielding of the bolt had occurred, showing that any plastic deformation redistributes the load. Fukuoka and Nomura (2008) proposed a novel method for analyzing threads in a finite element model that can take contact pressure and circumferential variation into effect. Aryassov and Petritshenko (2008) studied the distribution of stresses in bolt threads using mathematical approximations that closely matched finite element analyses performed in previous research. Finite element analysis of fatigue is another novel area of research, as shown by Carlyle and Dodds (2007), who demonstrated that crack closure in fully reversed fatigue loading can be modeled successfully.

## CHAPTER 3 EXPERIMENTAL PROCEDURES

### 3.1 SPECIMENS

All CDA 360 brass notched specimens were provided by Mr. Christopher Hahin of the Illinois Department of Transportation, designer of the device.

#### 3.1.1 Bending Tests of Design 1

The notched surface and one flat exterior face of the hexagonal brass couplings were prepared for mounting strain gages by sanding the brass surfaces with 180-, 240-, and 400-grit sandpaper. An acid etching solution was first applied to the prepared surfaces on the brass couplings, and then de-ionized water was applied to create an acceptable surface for mounting the strain gages. Two strain gages (Vishay EA-13-031EC-120, EA-13-125BZ-350) were bonded onto each coupling. One strain gage was applied in the root of the notch and one on the flat surface of the hexagonal bar (Figure 3).

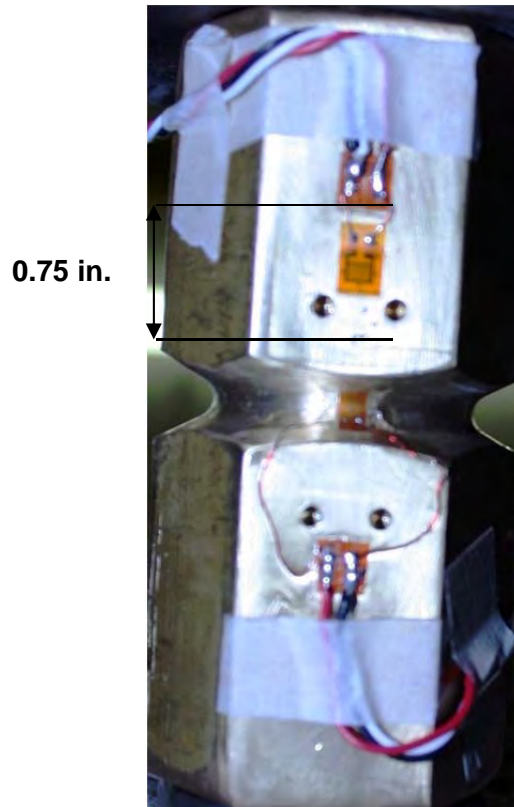


Figure 3. Strain gage placement.

#### 3.1.2 Monotonic Tests

Tensile specimens were fabricated from 1 in. hexagonal CDA 360 brass obtained from McMaster-Carr Supply Company. Machining and polishing were performed by Wagner Machine Co. of Champaign, Illinois. A small sample of the hexagonal bar ordered from McMaster-Carr was sent to Chicago Spectro Services Lab for chemical analysis to ensure the material was within the specifications for free-cutting brass set by ASTM Standard B16-10 (2010). Dimensions for the tensile specimens are illustrated in Figure 4. The chemical composition of the sample is shown in Table 1.

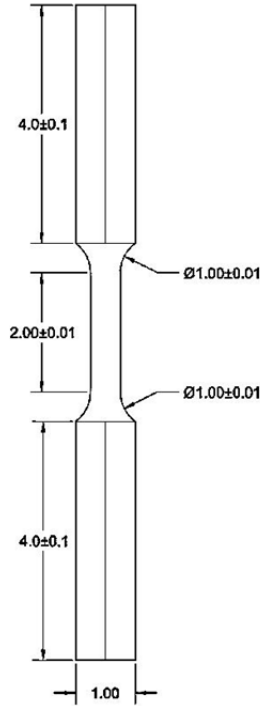


Figure 4. Tensile specimen geometry (in.).

Table 1. Chemical Composition for CDA 360

Element	Analysis	ASTM B16
Copper (%)	60.07	60.0–63.0
Lead (%)	2.76	2.5–3.7
Iron (%)	0.27	< 0.35
Zinc (%)	Balance (36.6)	Remainder
Manganese (%)	0.01	...
Nickel (%)	0.10	...
Tin (%)	0.19	...

“...” Indicates that there is no requirement.

### 3.1.3 Fatigue Tests of Design 1

The notched surface and one of the flat faces of the hexagonal brass couplings were prepared for strain gages by sanding with 180, 240, and 400 grit sandpaper. An acid etching solution was applied to the prepared surfaces on the brass coupling, and then de-ionized water was applied to neutralize the acid. Two strain gages (Vishay<sup>®</sup> EA-13-031EC-350, EA-13-125BZ-350) were attached onto each coupling. One was attached onto the flat surface and the other in the notch root (Figure 3). Two strain gages were used for the first five tests performed, during which the effect of bending stresses were noted. Afterward, six gages were applied to the two remaining couplings to determine bending stresses induced by the testing parameters.

### **3.1.4 Bending Tests of Design 2**

Three of the flat faces of the hexagonal brass couplings were prepared for strain gages by sanding with 180, 240, and 400 grit sandpaper. An acid etching solution was applied to the prepared surfaces on the brass coupling, and then de-ionized water applied to neutralize the acid. Six strain gages (Vishay® EA-13-125AC-350) were attached onto each coupling, one on each of the prepared flat surfaces.

### **3.1.5 Fatigue Tests of Design 2**

The method of strain gage preparation was the same as used in the bending tests of Design 2.

### **3.1.6 Fatigue Testing of Design 2 with Salt Spray**

A set of four couplings of Design 2 were subjected to a salt spray bath for 1000 hr in accordance with ASTM Standard G85 prior to fatigue testing. The salt and corrosion products were removed with a power sander, and then the same method of preparation was used as described in Section 3.1.4.

## **3.2 TESTING SETUP**

### **3.2.1 Bending Tests of Design 1**

Prior to assembly of the testing system, it was noted that the concrete base provided had to be altered to allow fitting of testing equipment. The concrete base was attached to a concrete testing wall using a specially made steel plate (Figure 5). A small amount of concrete was chipped off the base around one of the protruding studs to allow placement of a locking nut (Figures 6 and 7). A specially fabricated steel plate was made for this test and then attached to the strong wall on the east end of the Newmark Structural Engineering Laboratory, as shown in Figures 8 and 9. Four steel rods were screwed into the tapped holes on the steel plate. The concrete foundation block was positioned onto the steel rods and clamped down to the steel plate using steel washers and nuts. A steel nut was screwed onto each of the four steel rods cast into the concrete foundation block. The hexagonal brass couplings were then screwed onto the same rods as the steel nuts to a nominal depth of 1.5 in., aligning the strain gages to form a vertical plane, and made parallel with the direction of loading. The steel nuts and hexagonal brass couplings were tightened to a nominal torque of 50 ft-lb against each other. The steel loading tube was placed onto the exposed stainless steel rods from the hexagonal brass couplings. A stainless steel nut was fastened onto each remaining stainless steel threaded rod that was thread-locked to each hexagonal brass coupling, and then torqued to 50 ft-lb.

A Simplex RK1001A 100 ton hydraulic actuator, equipped with a Moog Model 72-234C servo-valve, a  $\pm 5$  in. linear variable differential transformer (LVDT), and a calibrated 60 kip load cell, was placed underneath the loading tube, with a loading plate between the top of the actuator and the load cell. A roller pin was placed between the loading plate and the loading tube (Figures 7 and 8). An MTS® Hydraulic Service Manifold (HSM) was attached between the actuator and MTS® Hydraulic Power Supply. Both the actuator and the HSM were driven by an INSTRON® 8500 Plus controller.

Brass couplings were tested in three different configurations: diamond, square, and individually loaded. For the square orientation, refer to Figure 8; for the diamond orientation, refer to Figure 9, and for the individually loaded orientation, refer to the Results section of this report.

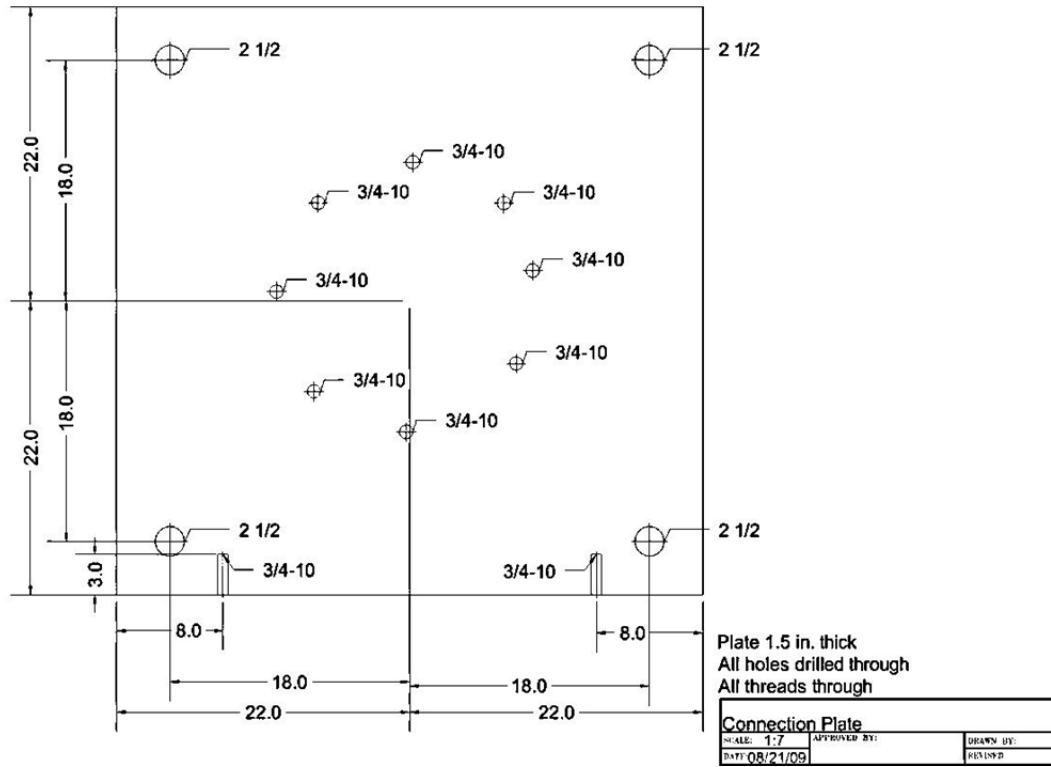


Figure 5. Loading plate design.



Figure 6. Concrete block before chipping.



Figure 7. Concrete block after chipping.

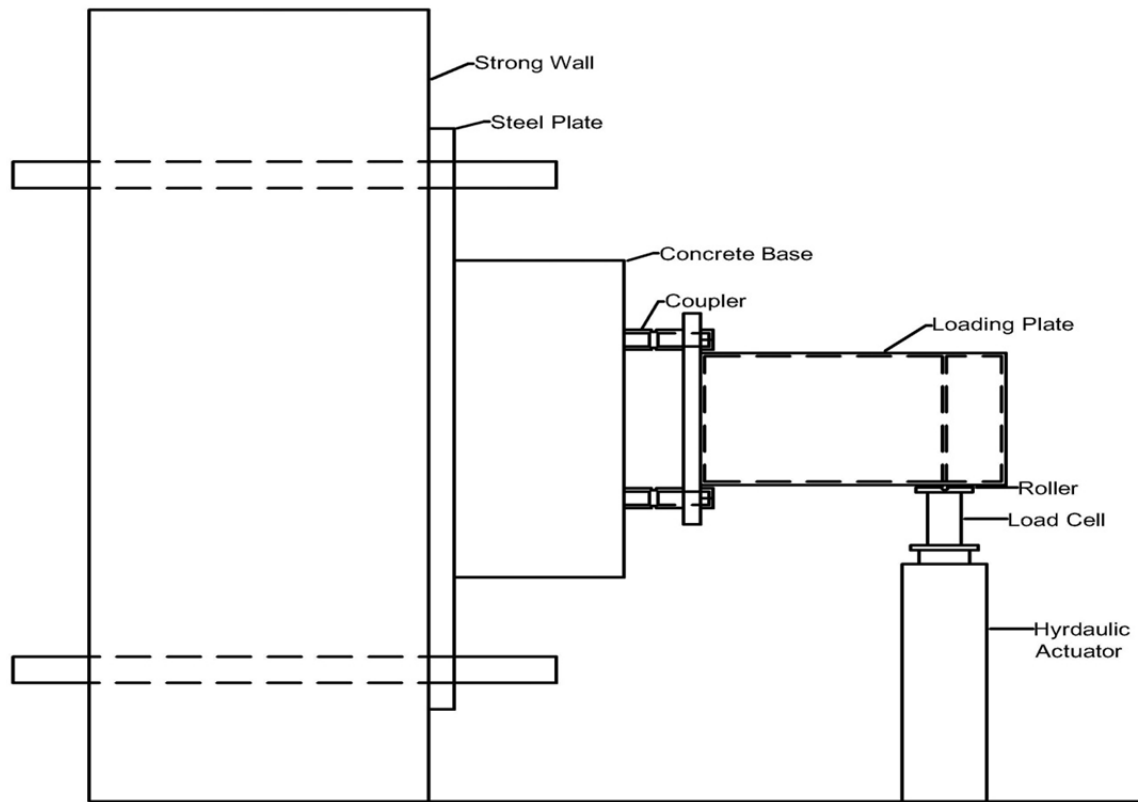


Figure 8. Square loading configuration.

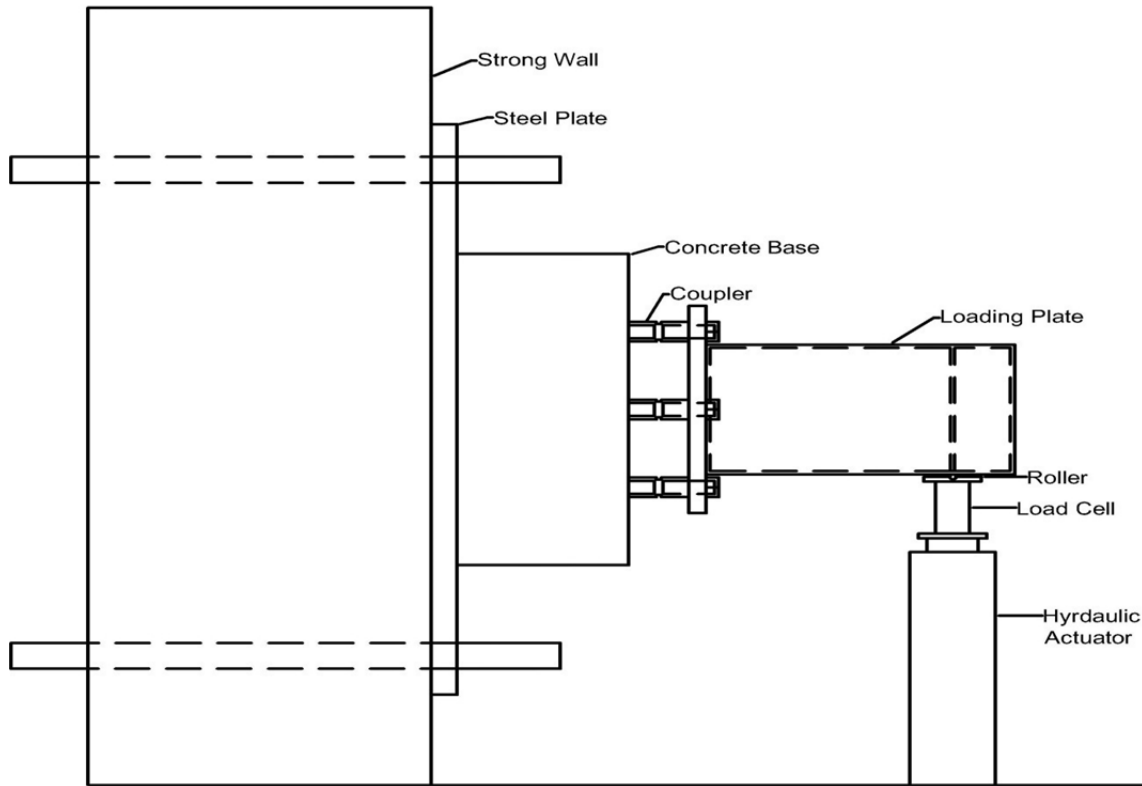


Figure 9. Diamond loading configuration.

### 3.2.2 Monotonic Tests

An MTS® 50 kip testing frame was driven by an Instron® 8500 Plus controller. Tension testing was performed using the mechanical grips of the testing frame only.

### 3.2.3 Fatigue Tests of Design 1

The MTS® 50 kip testing frame was driven by an Instron® 8500 Plus controller. Two cylindrical extension grips were specially made to attach the couplings to the MTS® 50 kip testing frame. The design of these extension grips can be seen in Figure 10 (next page).

### 3.2.4 Bending Tests of Design

An MTS® 11 kip testing frame driven by an Instron® 8800 controller was used. A modified angle plate was used to secure a single coupling to the frame, and the extension grips made for the 50 kip frame were attached to the exposed end of the coupling.

### 3.2.5 Fatigue Tests of Design 2

The testing setup used was identical to the fatigue tests of Design 1.

### 3.2.6 Fatigue Tests of Design 2 with Salt Spray

The testing setup used was identical to the fatigue tests of Design 1.

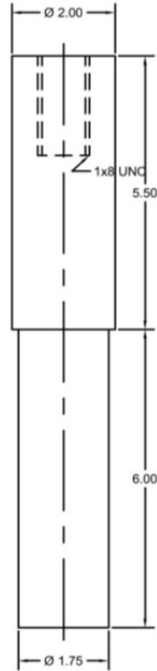


Figure 10. Fatigue grips (dimensions in inches).

### 3.3 TESTING PROCESS

All testing was performed under laboratory conditions. The temperature was 72 °F with a controlled relative humidity of 30%.

#### 3.3.1 Bending Tests of Design 1

Specimens in each orientation were tested in the elastic range up to a maximum strain of 724  $\mu\epsilon$ , which was measured at the root of the notch. Tests were carried out in force-control mode using a single ramp function at a rate of 1 kip/min. A Lab View®-based data logger was used to monitor each test.

#### 3.3.2 Monotonic Tests

Chemical analysis of the hexagonal brass specimen confirmed that it conformed to ASTM Standard B16 for the chemical composition of CDA 360 free-cutting brass. The results of the chemical analysis are compared with ASTM requirements in Table 1. The tensile specimens were pulled to fracture in tension under displacement control at 0.1 in/min prior to yielding and 1 in/min after yielding. Each specimen was inserted and then tightened to the top mechanical grip. The lower end of the specimen was inserted and then tightened into the lower mechanical grip. The alignment head was also tightened. The attached Instron® 2 in. extensometer was removed near its maximum effective range, and the data from the linear variable differential transducer (LVDT) mounted in the actuator were used to approximate post-yielding behavior.

#### 3.3.3 Fatigue Tests of Design 1

Fatigue testing was performed in force control in full compression-tension reversal ( $R = -1$ ) at a frequency of 10 Hz using a sine wave with constant amplitudes of 4.25, 4.5, 5.0, and 5.5 kips. Couplings were fastened to each extension grip at a torque of 100 ft-lb to ensure that no slip occurred during testing. The top extension grip was inserted into the top

mechanical grip, and the mechanical grip was tightened. The crosshead was then lowered to place the bottom extension grip into the bottom mechanical grip. The bottom mechanical grip was then pressurized. After the bottom grip was pressurized, the alignment head was pressurized, and the test started. If the specimen did not fail after  $N = 10^7$  cycles, the test was terminated and called a run-out. ASTM Standard E 1012 (2005) was followed to determine bending stresses using these testing parameters.

#### **3.3.4 Bending Tests of Design 2**

A single specimen was loaded at a distance of 0.75 in. from the notch, and testing was terminated at a clip gage reading of 0.0001 in. movement, which was a strain of 0.1%. Tests were carried out in force-control mode using a single ramp function at a rate of 1 kip/min. A Lab View®-based data logger was used to monitor each test.

#### **3.3.5 Fatigue Tests Design 2**

Fatigue testing was performed in force control in full compression-tension reversal ( $R = -1$ ) at a frequency of 10 Hz using a sine wave with constant amplitudes of 5.0, 5.5, and 5.7 kips. The remainder of the procedure was the same as the fatigue testing for Design 1.

#### **3.3.6 Fatigue Tests of Design 2 with Salt Spray**

Testing was performed under the same conditions used in the fatigue tests of Design 2 with loads of 5.0 and 3.75 kip.

## CHAPTER 4 RESULTS AND DISCUSSION

### 4.1 BENDING TESTS DESIGN 1

The measured strain was plotted against the calculated theoretical strain for the square, diamond, and individual loading cases, which can be seen in Figures 11, 12, 13, and 14. In Figures 11 and 12, strain in the notch area and on the side of the hexagonal section was determined by loading the four couplings in a light pole base configuration. In Figures 13 and 14, the nominal strains on the side of the hexagonal section were compared with the notch strains when individual couplings were loaded in a test machine. Theoretical strain was determined from the moment of inertia and the parallel axis theorem for the full hexagonal section. Measured and calculated values of strain on the nominal section were recorded for a load that generated  $724 \mu\epsilon$  at the notch for all configurations (Table 2). An eccentricity was noticed following testing because the couplings were not equidistant from the loading wall due to irregularities in the concrete base. In any future second test, these couplings must be offset by an equal distance from the load frame wall by use of leveling nuts. Figure 15 shows the amount of eccentricity induced by the offset.

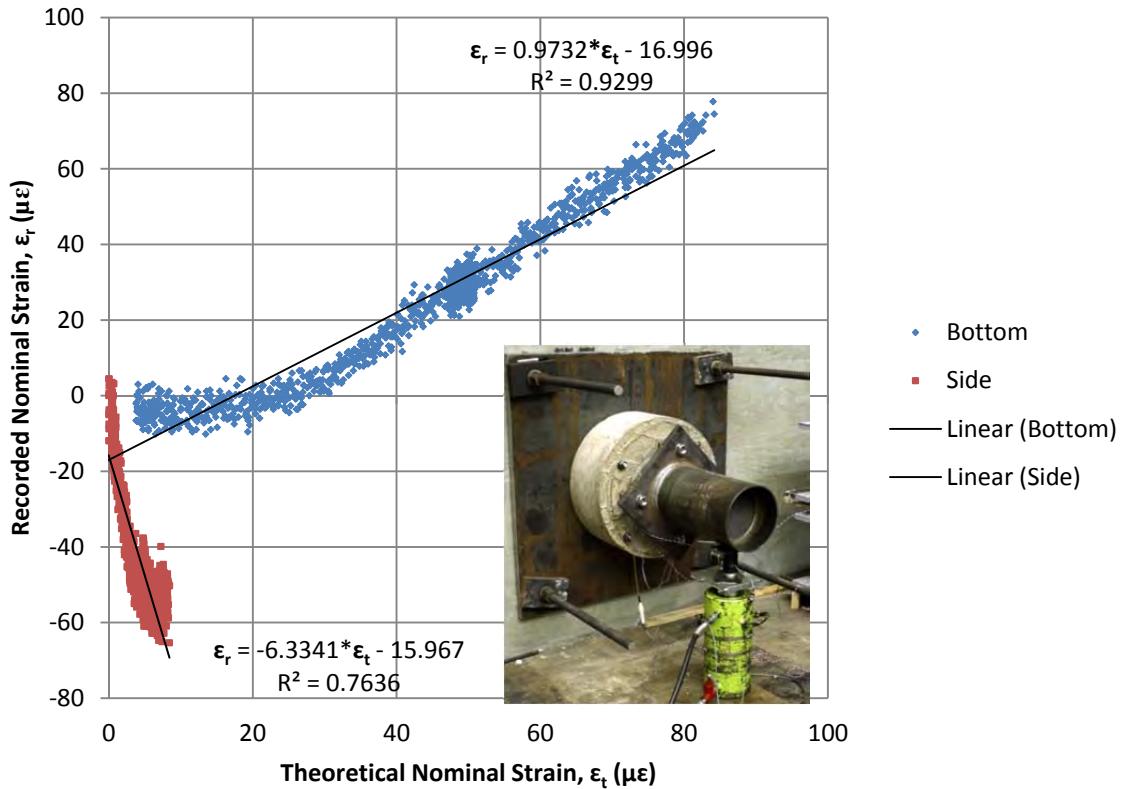


Figure 11. Theoretical vs. recorded strain in diamond configuration.

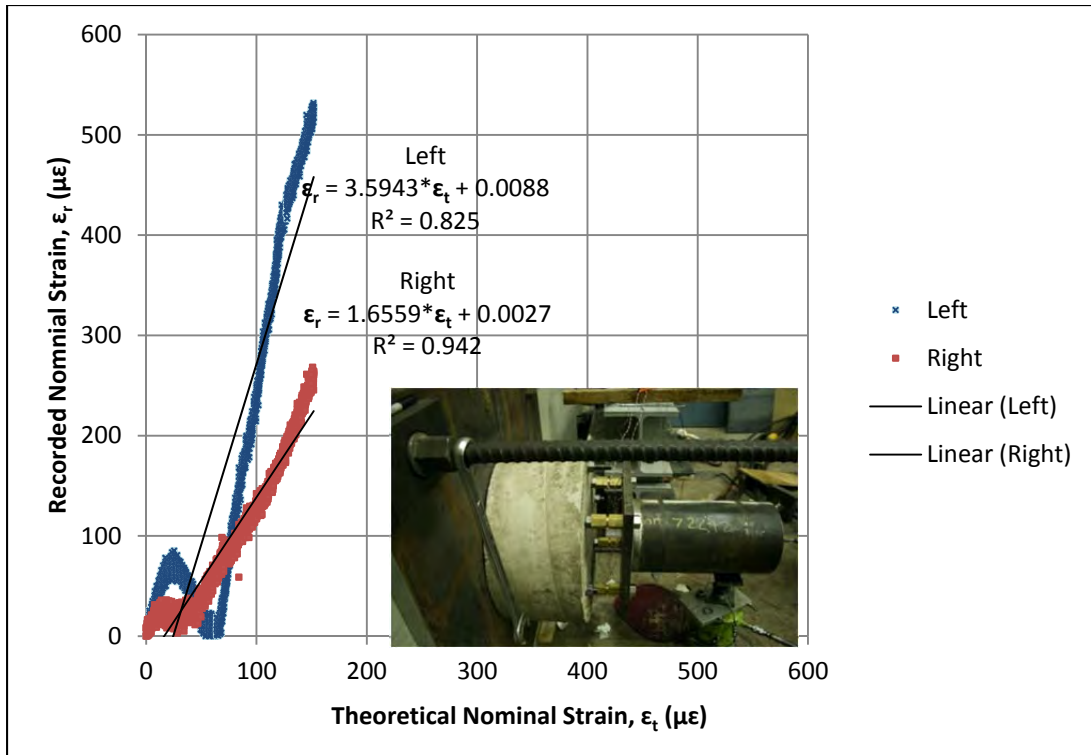


Figure 12. Theoretical vs. recorded strain in square configuration.

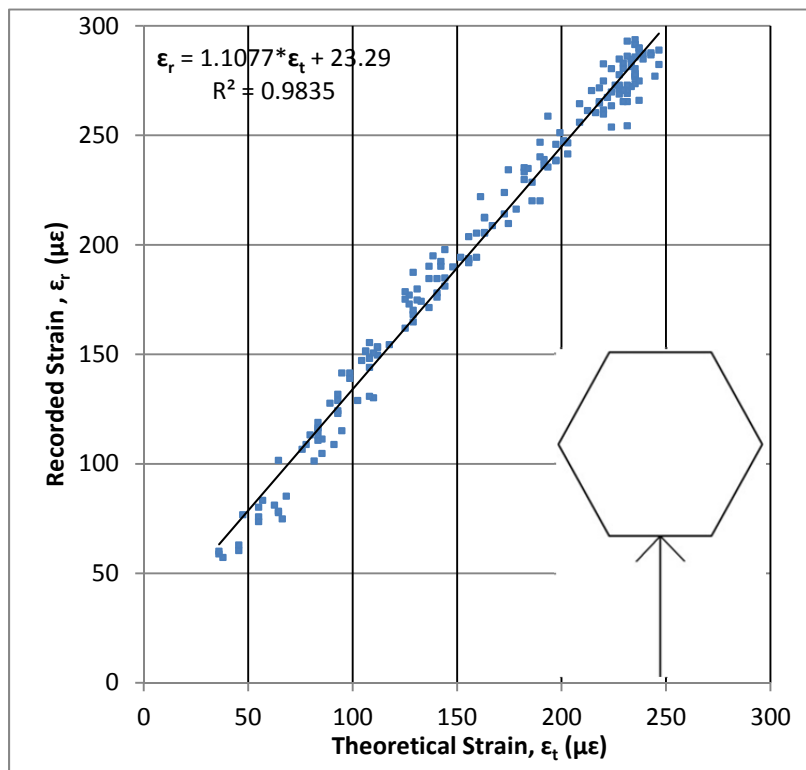


Figure 13. Theoretical vs. recorded strain loading of coupling 1.

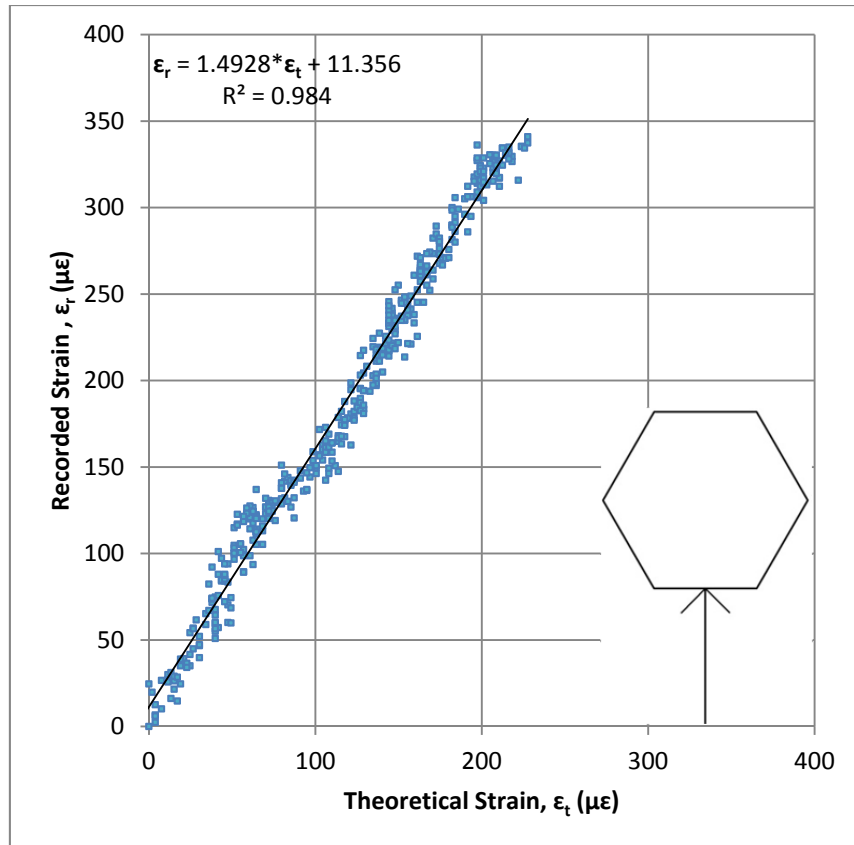


Figure 14. Theoretical vs. recorded strain loading of coupling 2.

Table 2. Nominal Strain at Notch Strain of 724  $\mu\epsilon$

Configuration	Force (kip)	Moment (in-kip)	Calculated Strain ( $\mu\epsilon$ )	Recorded Strain ( $\mu\epsilon$ )
Square	2.11	37.24	65.2	62.55
Diamond	1.98	35.7	86.5	77.16
Single Coupling #1	0.031	0.36	73.1	126
Single Coupling #2	0.038	0.446	78.7	106.2

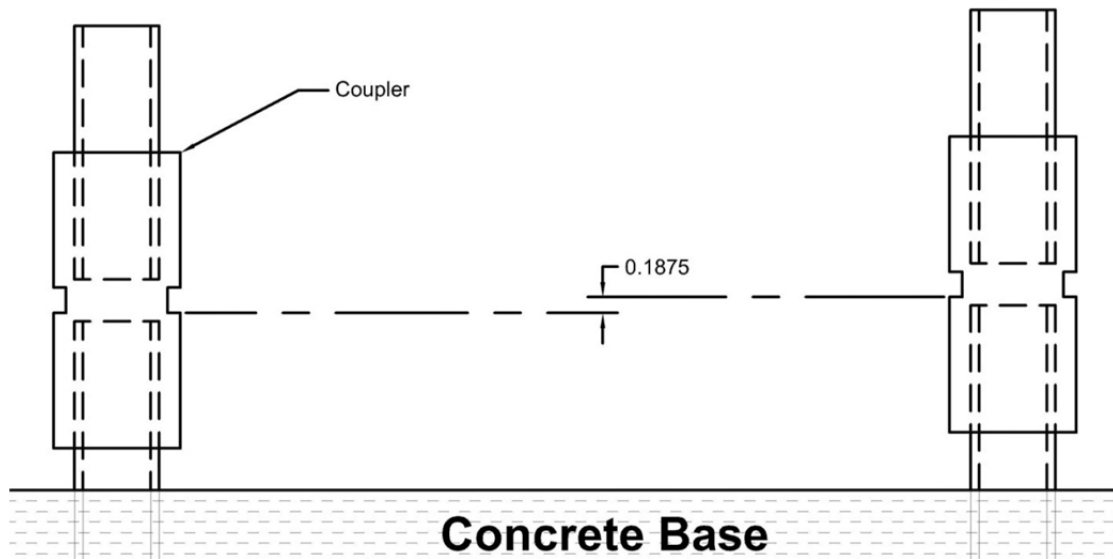


Figure 15. Eccentricity of couplings resulting from testing setup, in inches.

As can be seen in figures depicting the response of strain gages for the diamond and square configurations, the relationship between applied load and recorded strain was not entirely linear. The behavior is most clearly evidenced by the square configuration, in which the strain on the bottom left coupling began in tension, transitioned to compression, and back to tension at a very high rate of strain increase. This unexpected non-linearity is most likely due to the eccentricity in the couplings noted above.

Using data obtained during testing, the point at which the strain at the notch reached a value of  $724 \mu\epsilon$  was determined, and data were recorded for values of strain and force on the nominal section. The calculated strain, derived from the moment of inertia and the parallel axis theorem, and the recorded strains on the nominal section are similar for the square and diamond configurations. The lower observed value for the diamond configuration is likely due to the observed compression in the side coupling resulting from the eccentricity in the loading setup. Loading of individual couplings separately did not agree well with calculated values derived from the moment of inertia (a 24% difference), and the difference is most likely due to the high noise levels from the load cell present at such low force loadings.

The stress concentration factor,  $K_t$ , was defined as the ratio of the strain recorded at the notch divided by the strain at the full section, and was found to be 5.7. The theoretical stress concentration factor of 4.7 derived from the work of Peterson (1974) was 18% less than the actual recorded value.

#### 4.2 MONOTONIC TESTS

Tensile testing was performed to ensure accurate selection of fatigue testing stress levels and verify material properties. The yield stress was determined at 0.5% strain in accordance with ASTM Standard B16 (2010). Data obtained from tensile testing are presented in Figures 16, 17, and 18, as well as in Table 3. The average yield strength was 36,850 psi, and the average ultimate tensile strength was 57,100 psi. The non-linear shape of the stress-strain curve, coupled with limited fatigue data for similar brass alloys, guided the selection of loading cases for the fatigue study. Fracture surfaces of the tension

specimens were also compared with the fracture surface of the fatigue specimens to more easily identify the ductile fracture surfaces compared to the fatigue fracture zones.

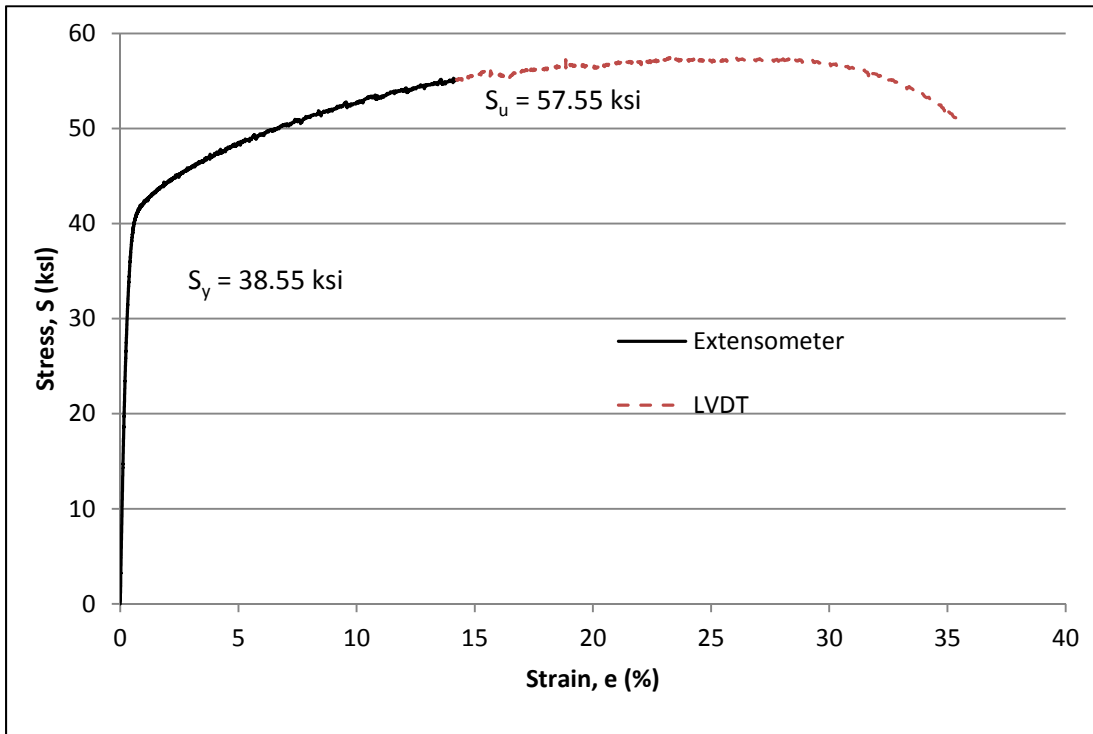


Figure 16. CDA 360 0.500 in. round tensile specimen 1.

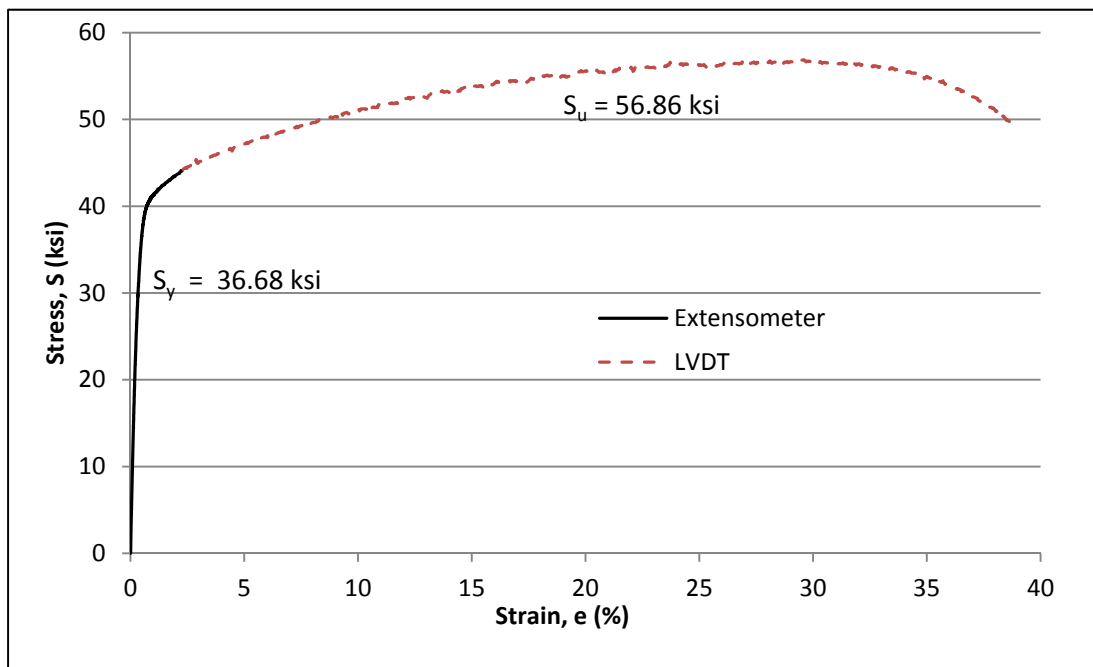


Figure 17. CDA 360 0.500 in. round tensile specimen 2.

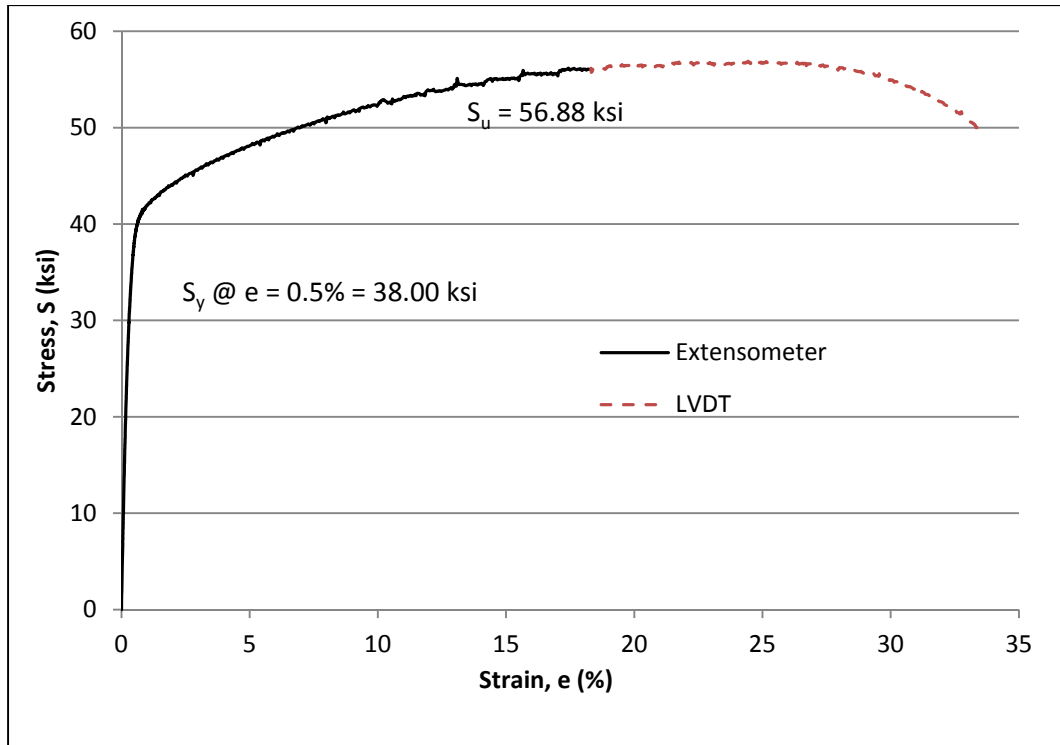


Figure 18. CDA 360 0.500 in. round tensile specimen 3.

Table 3. Material Properties of CDA 360

Specimen	1	2	3	Avg.	ASTM B16
Yield Stress (ksi)	35.88	36.68	38	36.85	$\geq 25$
Ultimate Stress (ksi)	57.55	56.86	56.88	57.10	$\geq 55$
Elongation (%)	35.6	37.9	33.6	35.7	$\geq 10$
Young's Modulus (ksi)	13,836	11,925	14,372	13,378	14,000*

\*Value from the ASM Handbook, Vol. 2, 10th Edition

### 4.3 FATIGUE TESTS DESIGN 1

Fatigue testing showed a substantial amount of scatter, as evidenced by the relatively modest coefficient of correlation ( $R = 0.556$ ) obtained by the method of least-squares. This level of correlation is common in fatigue data. The regression line and data points are displayed on a stress vs. number of cycles (S-N) diagram in Figure 19 and in Table 4. The notch strain range was calculated from the applied force, the cross-sectional area, and the stress concentration factor (see Equation 16 in the appendix ).

The data of Moore and Lewis (1931) for a similar copper alloy were used in our study as an approximate shape of the S-N curve in tension-compression for the CDA 360 brass. This approximation was used to choose stress levels and the corresponding testing loads. The effect of pre-strain, as studied by Mnif et al. (2010), may have played a factor in the fatigue results due to the high torque applied, which could have induced pre-strain into the couplings. Torque was applied to ensure that no slip occurred between the face of the

couplings and the grip. The level of pre-strain applied to the hexagonal section, however, was not recorded because the cracking always occurred in the notch, which was believed not to have been influenced by the pre-strain applied to the extremities of the couplings.

Initial fatigue testing of the notch was performed using only two strain gages per specimen. Because of the large variance in cycles to failure, the possibility that high bending was induced by the testing setup was considered. To capture the resulting bending stresses, the procedures of ASTM Standard E 1012 (2005) for circular specimens were followed, with three strain gages applied equidistantly around the cross-section. Six strain gages were applied to each of the last two specimens 120° apart from each other in the notches and on the corresponding flat faces on the hexagonal bar. Experimental  $K_{tt}$  and  $K_{tc}$  results and averages are shown in Table 5.

Table 4. Fatigue Results for Design 1 (Without Bending Stresses)

Coupling	Load (kip)	Nominal Stress (ksi)	Notch Stress (ksi)	Number of Cycles	Failure	# of Gages
5	4.25	4.36	31.19	9,999,982	N	2
6	5	5.13	36.69	3,374,143	Y	6
7	4.25	4.36	31.19	2,693,060	Y	2
8	4.25	4.36	31.19	1,787,125	Y	2
9	5	5.13	36.69	621,184	Y	2
10	4.5	4.62	33.03	4,391,223	Y	2
0	5.5	5.65	40.36	832,542	Y	6

Table 5. Stress Concentration Factors for Design 1

Trial	Axial Notch Strain ( $\mu\epsilon$ )	Axial Nominal Strain ( $\mu\epsilon$ )	$K_t$	Bending Stress (%)
Tension 1	1,290.69	172.53	7.48	48.8
Compression 1	-1,466.47	-221.35	6.63	49.2
Tension 2	1,700.85	232.75	7.31	11.3
Compression 2	-1,555.99	-227.86	6.83	15.8
Tension 3	1,250.00	179.04	6.98	47.0
Compression 3	-1,243.49	-179.04	6.95	42.5
Compression Average			7.26	
Tension Average			6.80	

Bending stresses of nearly 50% were recorded for two of the three cases, indicating that bending stresses were sufficiently high enough to affect fatigue performance. Because of the observance of bending stresses, the relationship of bending stresses for the first five tests cannot be precisely determined, which is why a calculated stress range was used in place of recorded strain gage data. In Figure 20, bending stresses for the first design were assumed to be the average of bending stresses recorded from all testing (37%), which is an estimation of actual testing conditions for each individual coupling.

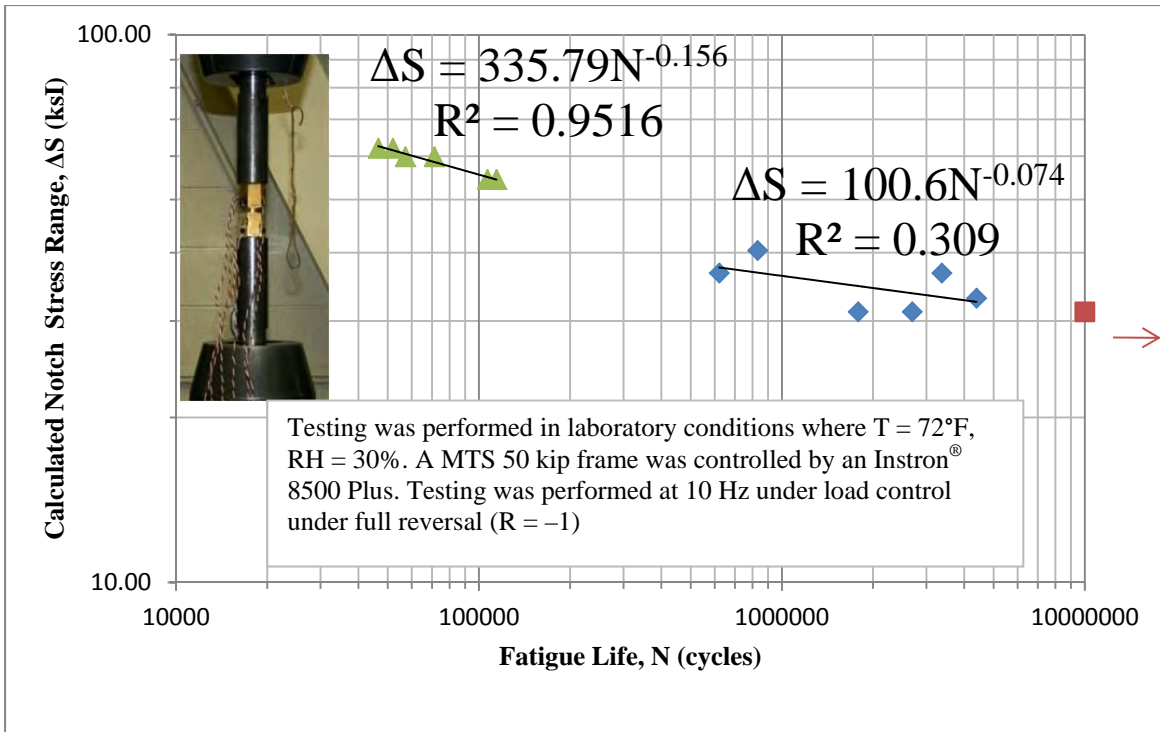


Figure 19. S-N curve of notched brass couplings (without bending stresses).

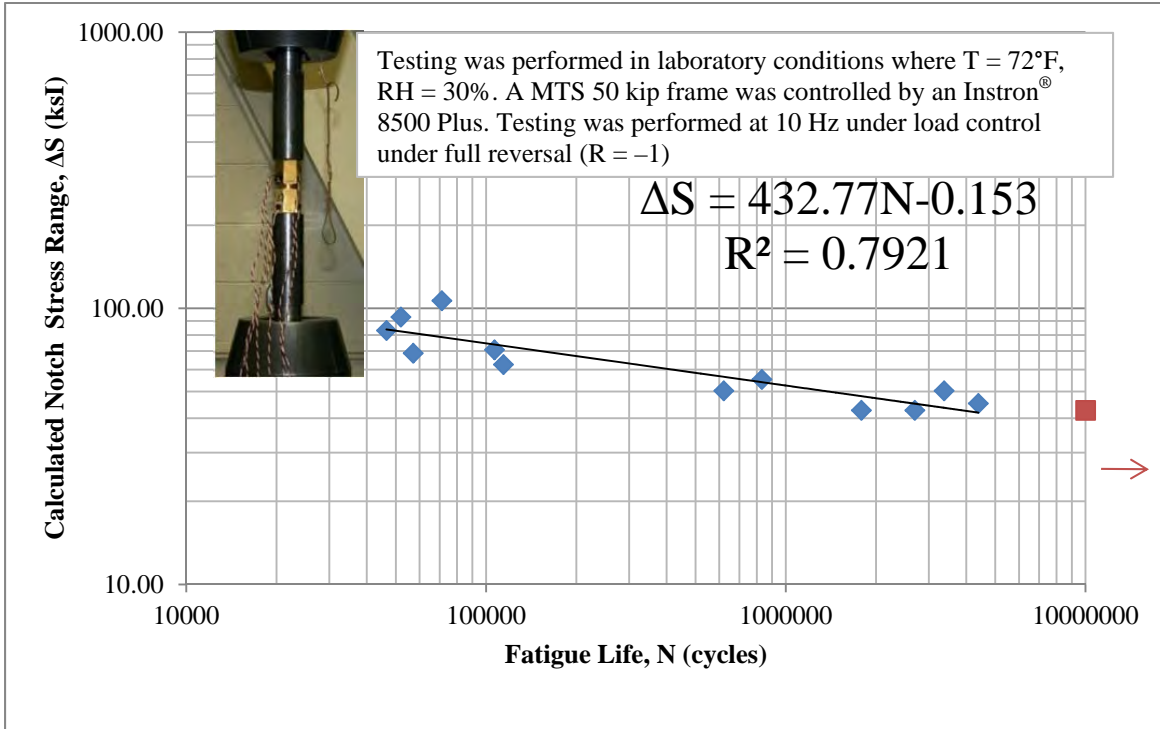


Figure 20. S-N curve of notched brass couplings (with bending stresses).

To determine a cause for high bending stresses, the frame, grips, and couplings were examined. The brass couplings were not drilled and tapped perfectly parallel with respect to the central longitudinal axis of the hexagonal bar (Figure 21 and Table 6). The eccentricity in drilling meant that the top and bottom faces of the coupling would have to be modified to seat the couplings perfectly flush with the testing grips. The applied 100 ft-lb of torque may have been sufficient to deform the faces and apply unintentional stresses to the couplings, but the effect of the applied torque was not experimentally determined. The eccentricity encountered also affected the reduced section. An uneven amount of material was present axially relative to the notch, and in the presence of bending stresses, the uneven cross-section would have led to an uneven distribution of stresses. The different levels of bending stress noticed while performing the elastic bending test confirmed that uneven amounts of material in the notch affects fatigue performance because significantly different bending stresses occurred depending on the rotation of the coupling. The thread-locked studs protruding from the couplings may also have been slightly canted because of the possible incidence of non-parallelism with respect to the central axis of the hexagon bar stock. Measurements to verify this assumption were insufficiently limited. Compared with the change in wall thickness at the notched section caused by the drilling eccentricity, canting of the stainless stud had only minor effects on the induction of bending stresses.

The limitations in testing equipment required that the tension-compression fatigue testing be performed in place of rotating-bending testing. The correlation between uniaxial and rotating-bending testing is related to applied stresses and specimen size, but it is non-linear (Crawford 1974; Grover et al. 1960). No published data were available to directly correlate the concentration of stresses associated with notched hollow cylinders to the geometry or material of the couplings in this testing program. There is a common pattern in published literature that uniaxial testing causes more fatigue damage than in rotating bending as shown in Figures 22 and 23 (Crawford 1974; Grover et al. 1960). Figure 23 is a comparison of fatigue life in rotating bending vs. axial tension Grover, et al. 1960 for CDA 365, a brass alloy of 60% Cu, 39.4% Zn, and 0.6% Pb—which is nearly identical to the composition of CDA 360. Because of bending stresses, slight eccentricities, defects in the brass and manufacturing variances, and ample ductility of CDA 360 brass, it should be noted that cracks do not always initiate at the thinnest point.

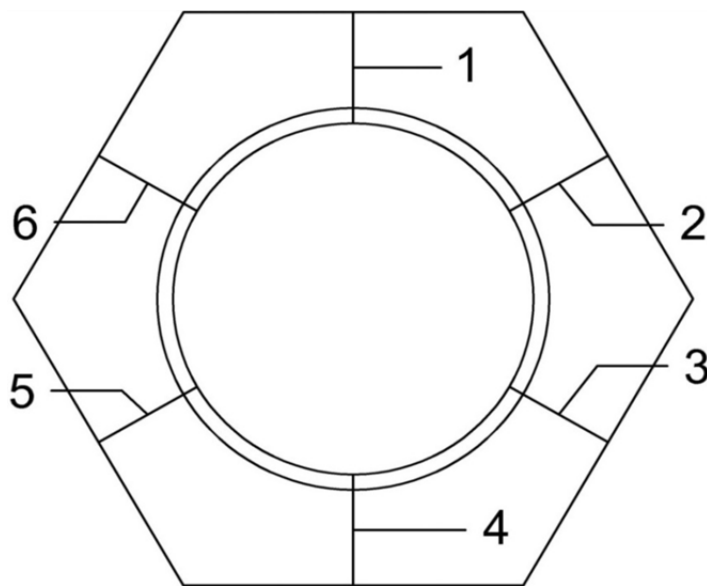


Figure 21. Coupling eccentricity measurement.

Table 6. Eccentricity in Couplings (in.)

Coupling	Side 1	Side 2	Side 3	Side4	Side5	Side6	Max/Min Difference
5 end	0.305	0.312	0.320	0.320	0.313	0.309	1.049
6 end	0.315	0.315	0.320	0.308	0.309	0.314	1.019
6 middle	0.311	0.314	0.310	0.310	0.313	0.314	1.013
7 end	0.309	0.312	0.317	0.314	0.311	0.306	1.036
7 middle	0.306	0.306	0.311	0.312	0.311	0.308	1.020
8 end	0.298	0.304	0.316	0.323	0.319	0.304	1.070
8 middle	0.304	0.304	0.311	0.316	0.311	0.311	1.039
9 end	0.307	0.310	0.317	0.316	0.314	0.305	1.039
9 middle	0.307	0.307	0.310	0.312	0.314	0.307	1.023
10 end	0.315	0.304	0.307	0.313	0.318	0.319	1.039
10 middle	0.310	0.306	0.307	0.311	0.313	0.314	1.026
0 end	0.313	0.323	0.323	0.309	0.296	0.299	1.080
0 middle	0.312	0.325	0.323	0.310	0.300	0.298	1.091

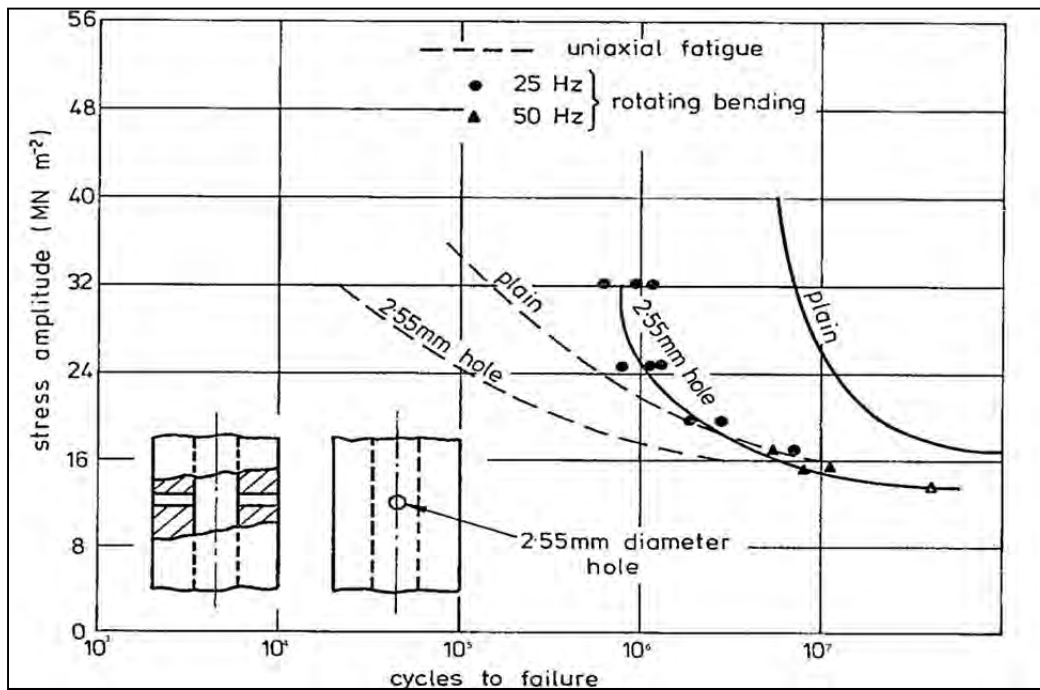


Figure 22. Comparison of uniaxial and rotating-bending fatigue of polymer (Crawford 1974).

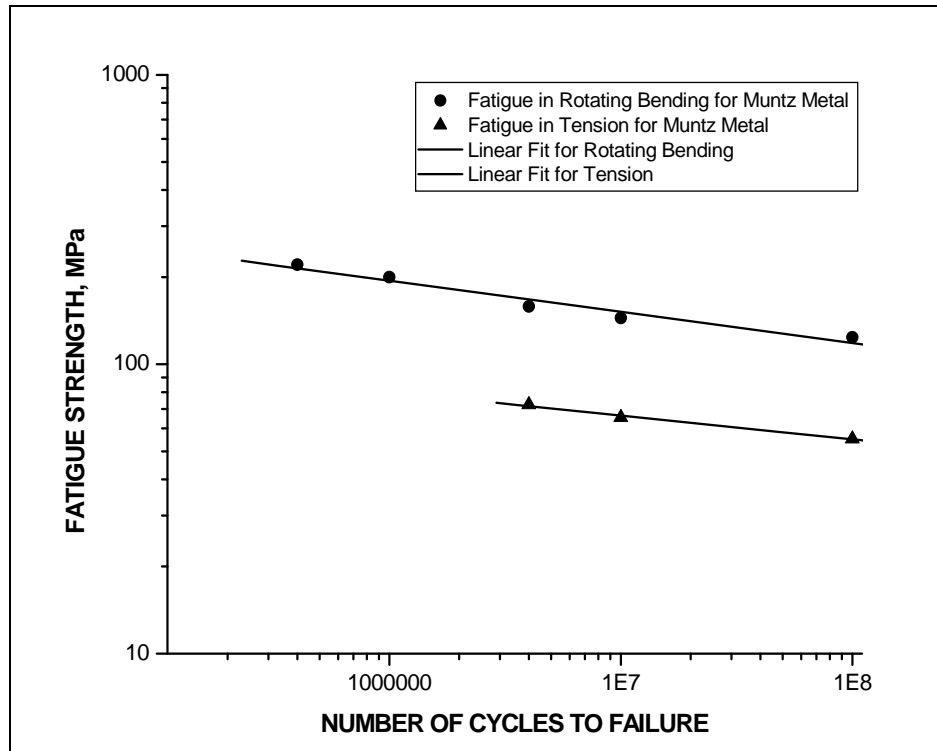


Figure 23. Comparison of uniaxial and rotating-bending fatigue of CDA 365 (Muntz Metal) (Grover et al. 1960).

#### 4.4 BENDING TESTS FOR DESIGN 2

The stress concentration factor in bending,  $K_{tb}$ , was found to be 9.0. Strain gages were unable to be applied in the notch as in Design 1 because of the deeper cut of the notch and the removal of the bevels above and below the notch cut. The deeper notch cut was intended to aid in their fracture in pendulum-impact certification tests. The removal of the bevels also reduced machining costs. The higher stress concentration factor resulted from the deeper cut of the notch compared with the first design. The high level of electronic noise from the extensometer across the notch requires the averaging of a large amount of data, and the determined stress concentration factor may not be perfectly precise. The level of electronic noise was noticeably higher using the 11 kip test frame compared with the 50 kip test frame, but the electronic noise problem was not resolvable during testing.

#### 4.5 FATIGUE TESTS FOR DESIGN 2

Because of the bending stresses induced by drilling and tapping the central hole of the hexagonal bar observed from fatigue testing of Design 1, each specimen had six gages attached to it to accurately determine bending stress levels. The tensile and compressive stress concentration factors were determined by use of the attached strain gages on the nominal section and an extensometer across the notch. The ratio of strain recorded by the extensometer to the strain measured by strain gages was used to determine the tensile and compressive stress concentration factors. The tensile  $K_{tt}$  was 10.40, and the compressive  $K_{tc}$  was 10.80. The bending stress levels for each coupling tested are shown in Table 7, and the fatigue performance is shown in Table 8 and in Figures 19 and 20.

Table 7. Bending Stresses Under Fatigue for Design 2

<b>Coupling</b>	<b>Load</b>	<b>Bending Stresses (% of Loading)</b>
41	5.50	78
42	5.00	15
43	5.70	50
44	5.70	34
45	5.00	30
46	5.50	15
Average		37

Table 8. Fatigue Results for Design 2 (Without Bending Stresses)

<b>Coupling</b>	<b>Load (kip)</b>	<b>Nominal Stress (ksi)</b>	<b>Notch Stress (ksi)</b>	<b>Number of Cycles</b>	<b>Failure</b>
41	5.50	5.65	59.84	71200	Y
42	5.00	5.13	54.40	114289	Y
43	5.70	5.85	62.02	51985	Y
44	5.70	5.85	62.02	46514	Y
45	5.00	5.13	54.40	106665	Y
46	5.50	5.65	59.84	57178	Y

A lower fatigue life testing range was used for the second design because of time and cost constraints. The fatigue behavior observed with the lower fatigue life range may not be directly comparable with the higher fatigue testing range, but an insufficient amount of couplings was tested to verify the compatibility of the two data sets. The results for the first and second designs are aggregated in Figure 20 with the addition of bending stresses recorded for Design 2 and the average of recorded bending stresses used for Design 1. The high correlation indicates that the combination of the two sets of data is valid and that the notch zone stress is the controlling variable in fatigue life. The second design shows a higher sensitivity than the first design to the applied stress range, as evidenced by the larger exponent value (-0.156 vs. -0.074). The higher sensitivity to the applied stress range could be an error in fatigue testing, or it could be a difference resulting from the variability of the wall thickness of the notched sections and the respective acuity of the notch. Extrapolation to higher cycle ranges as studied in the fatigue behavior of the first design shows similar allowable stress levels for the same fatigue life, which is to be expected of a very similar design with only a marginally deeper notch. The two designs were combined in a single graph representing fatigue life by use of the peak calculated notch stress range (Figure 19). The applied force was divided by the nominal cross-sectional area and multiplied by the stress concentration factor and then by the percentage of bending stresses determined from strain gage measurements (Table 7).

#### 4.6 FATIGUE TESTS DESIGN 2 WITH SALT SPRAY

Four of the brass couplings of Design 2 were subjected to 1000 hr of a salt spray bath in accordance ASTM Standard G85 and then tested in fatigue. The extent of corrosion was minimal: more salt solids than corrosion products accumulated. The first coupling failed prematurely from an equipment fault caused by a momentary loss of power. The failure occurred at 15,649 lb. The remaining three specimens showed no significant difference in fatigue life compared with those not subjected to a salt spray bath. No clear indications of

crack initiation sites were found on these three specimens. Fatigue results for the couplings subjected to salt spray testing are shown in Figure 24 and Table 9.

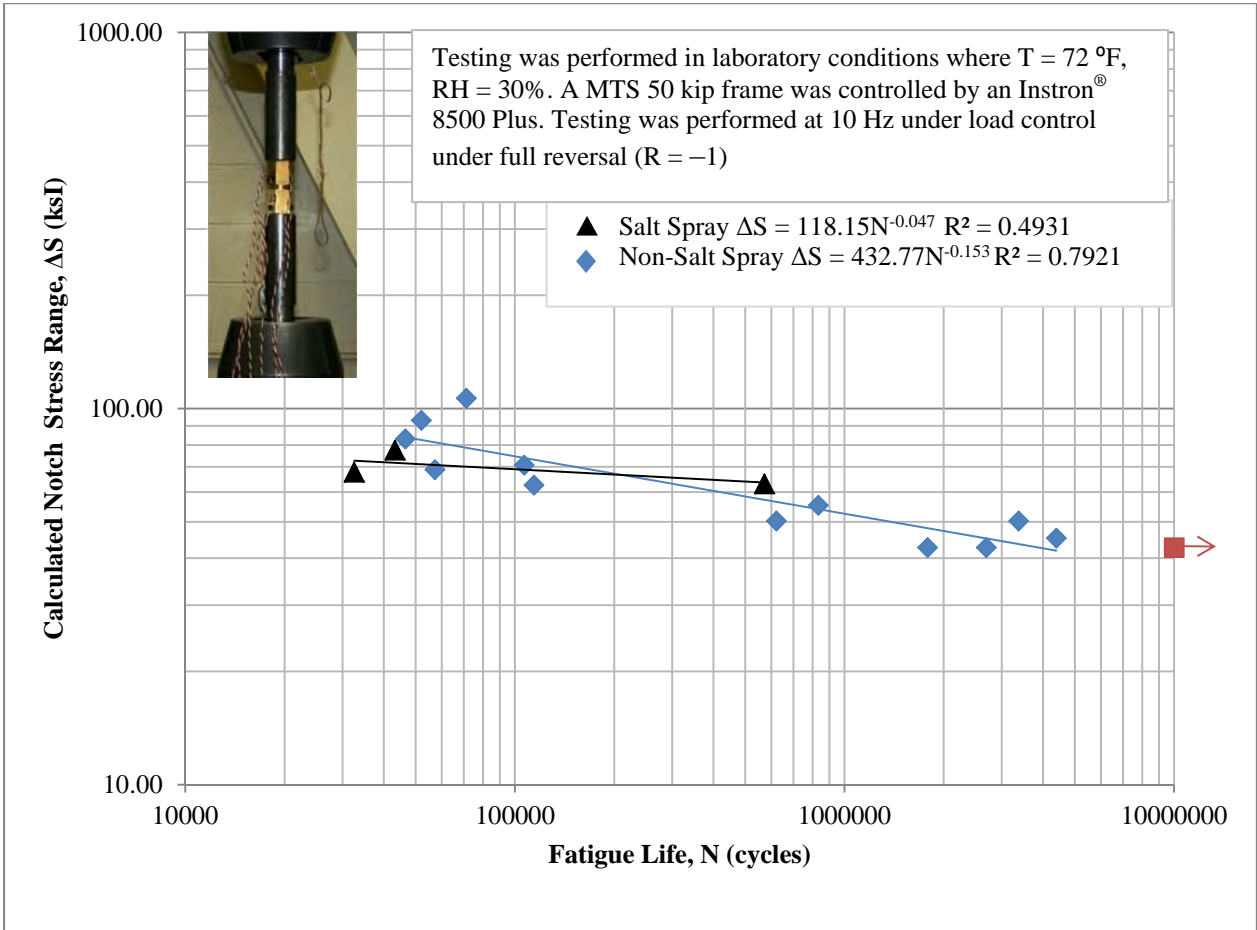


Figure 24. S-N curve of notched brass couplings (with bending stresses).

Table 9. Fatigue Performance of Couplings Suggested to Salt Spray

Coupling	Load (kips)	Nominal Stress (ksi)	Notch Stress Range (ksi)	Number of Cycles	Failure	Bending (%)
52	5.00	6.39	67.73	32,535	Y	24.5
53	5.00	7.32	77.58	43,265	Y	42.6
54	3.75	5.95	63.08	571,163	Y	54.6

#### 4.7 FRACTURE SURFACE ANALYSIS

Macroscopic examination of the fracture surfaces was performed for all fatigue specimens. Low magnification pictures of the fracture surfaces can be seen in Figures 25 through 41. All cracks appear to have originated from the internal threads of the couplings, and from a single location area, which is indicated by the use of magnified sections. Cracks initiated from the internal threads because of the sharper notch compared with the external notch and were expected because of the higher theoretical  $K_t$  of 10.0 (Peterson 1974). Crack initiation from the internal threads was verified in slow-strain rate tensile rupture tests at BMPR; rupture from pendulum impact at the Valmont test site located in Valley, NE; and in drop-weight impact tests conducted at Taylor Devices located in North Tonawanda, NY. The typical beach marks of fatigue specimens are not easily perceived in the photographs of the fracture surface because the camera equipment used had a limited depth of field, but they are present and visible on the actual couplings at higher magnifications. The fatigue crack zone is at most roughly one-quarter of the circumferential surface between the inner and outer diameter of the notch. The area of initiation occurs at defect zones in the internal threading. These defects are microscopic and cannot be discerned at the low magnifications used in Figures 25 to 41.

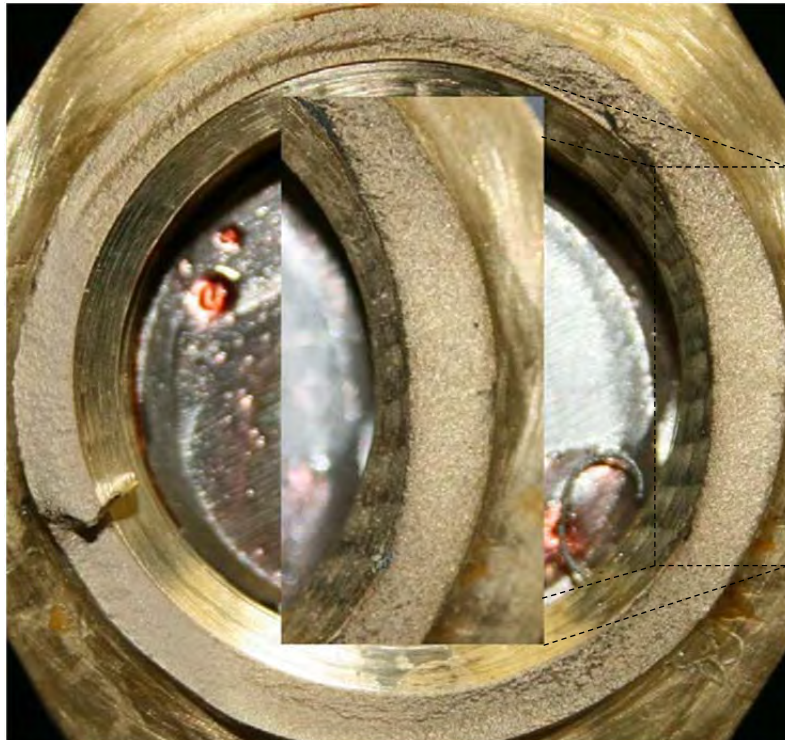


Figure 25. Fracture surface of coupling 6.

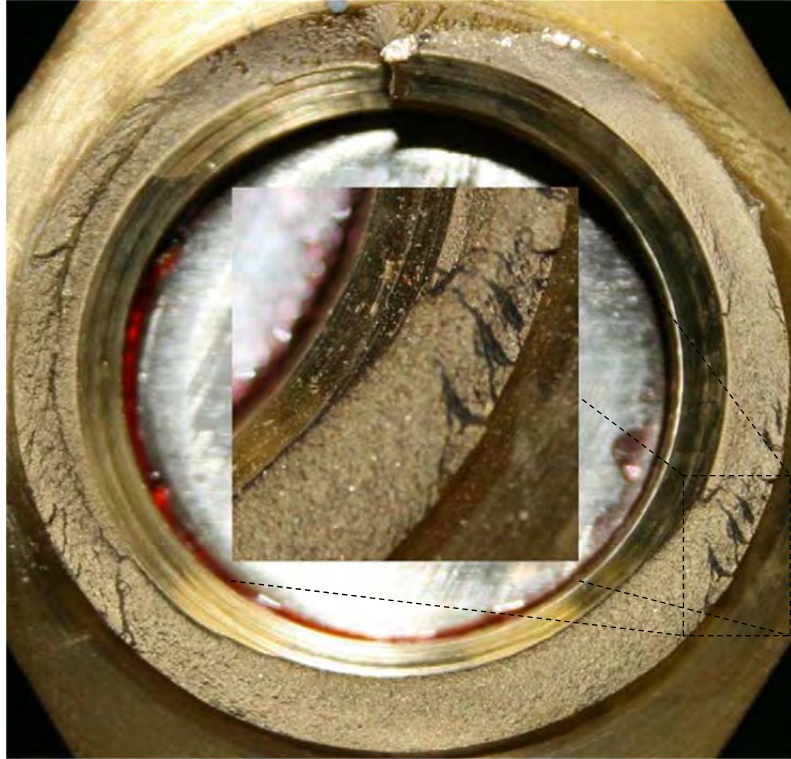


Figure 26. Fracture surface of coupling 7.

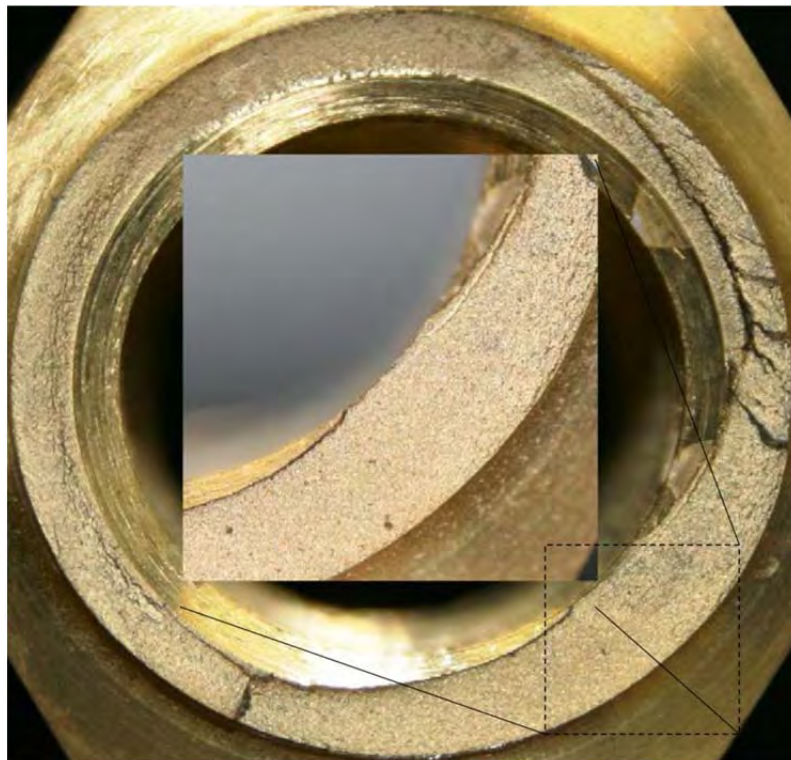


Figure 27. Fracture surface of coupling 8.

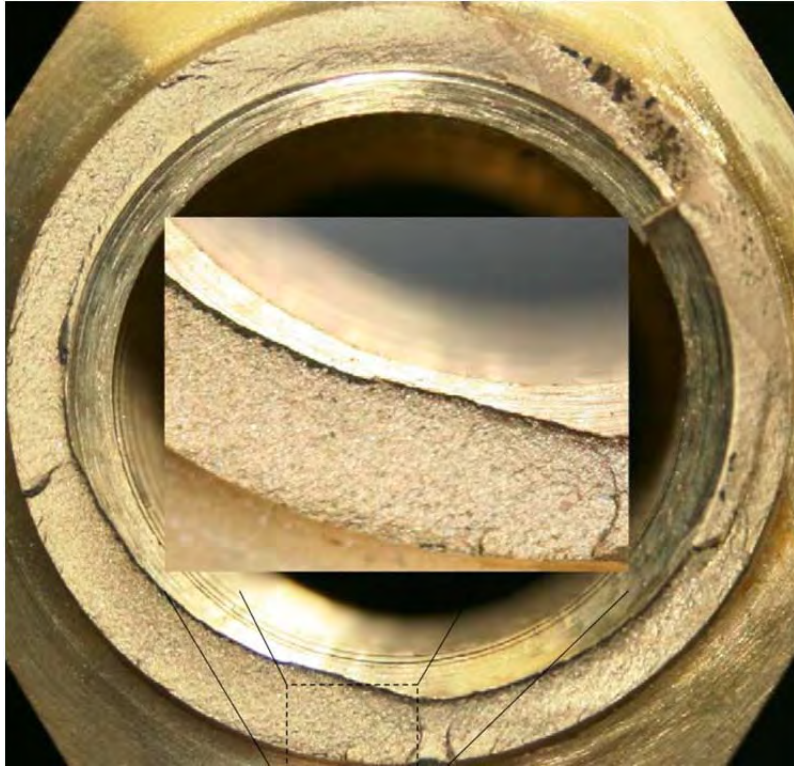


Figure 28. Fracture surface of coupling 9.

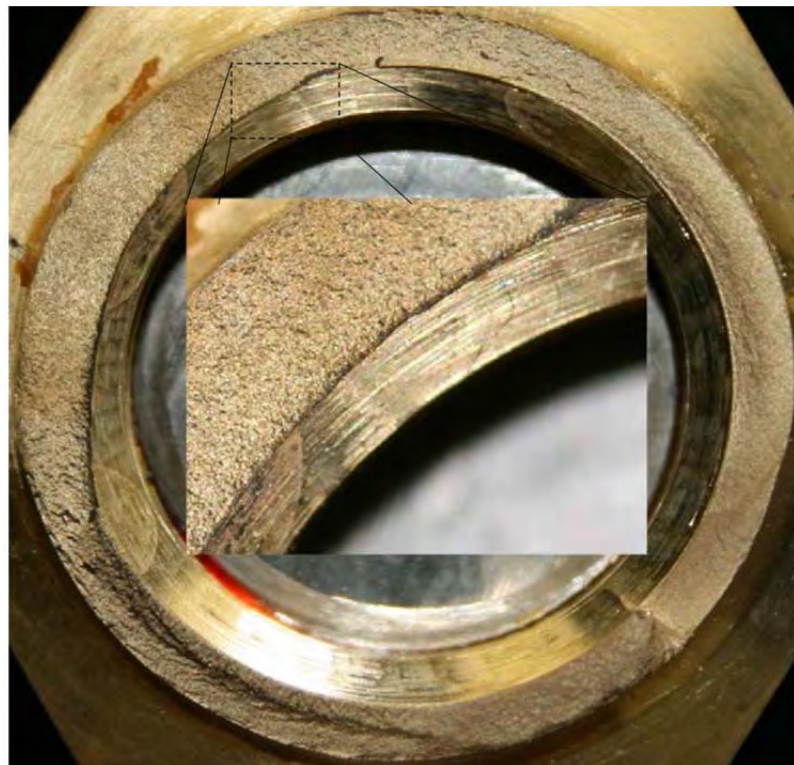


Figure 29. Fracture surface of coupling 10.

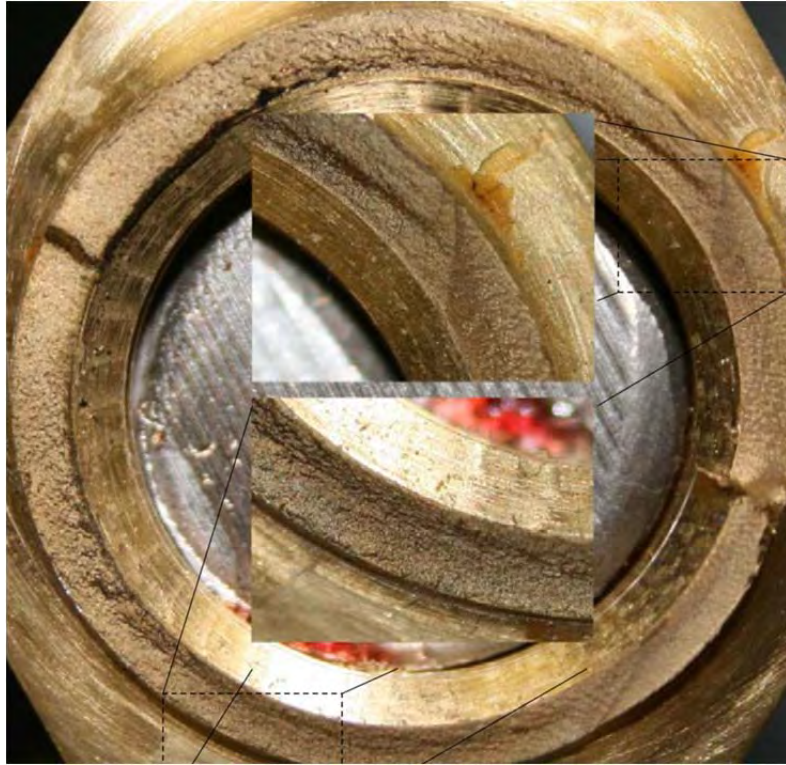


Figure 30. Fracture surface of coupling 0.



Figure 31. Fracture surface of coupling 31.

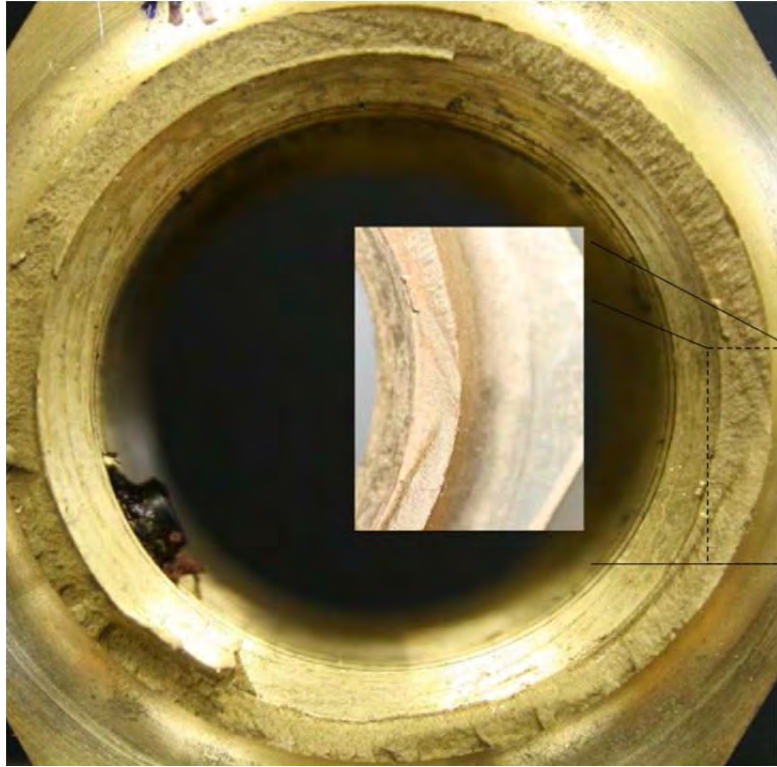


Figure 32. Fracture surface of coupling 41.

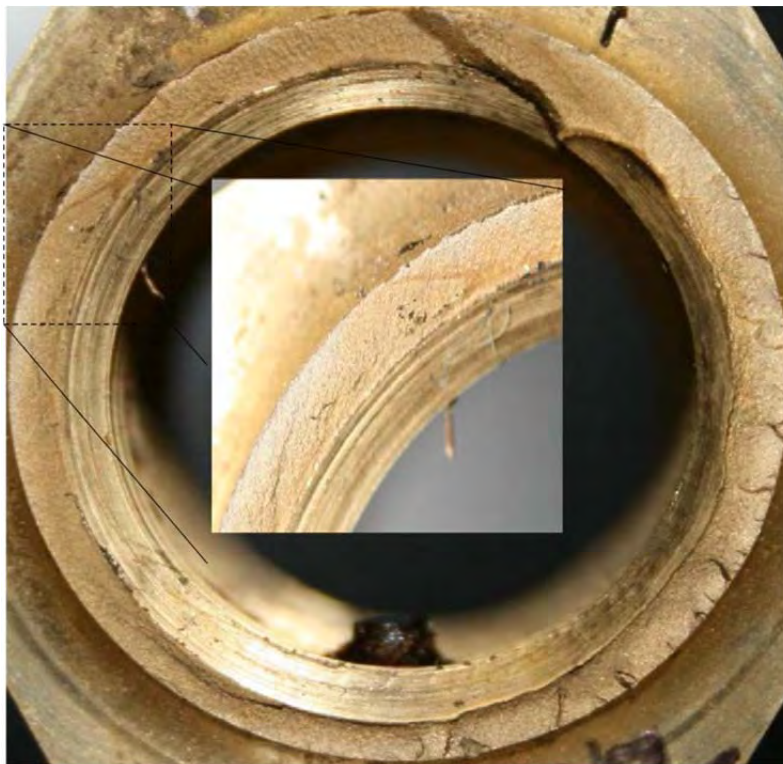


Figure 33. Fracture surface of coupling 42.

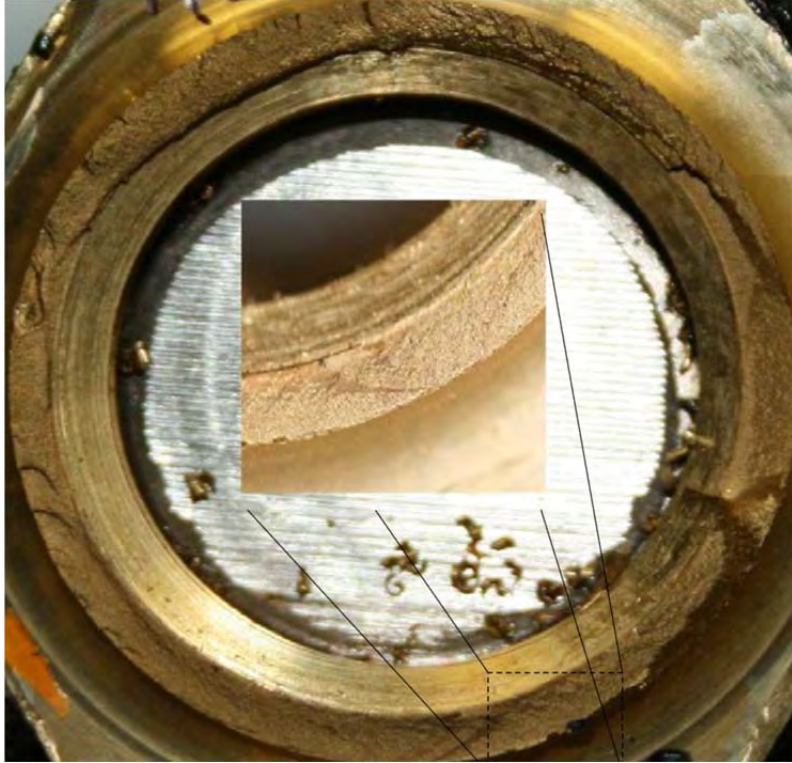


Figure 34. Fracture surface of coupling 43.

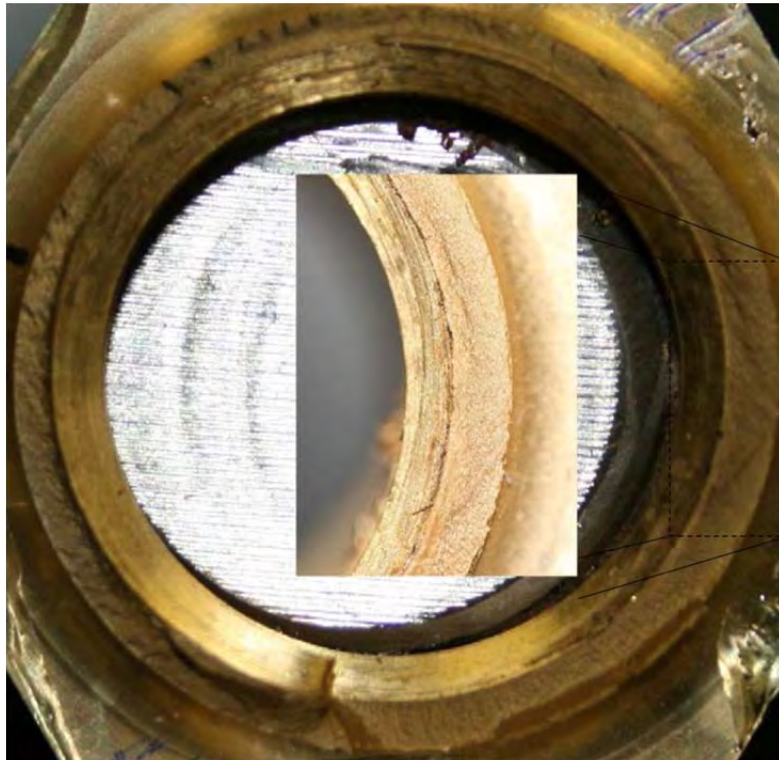


Figure 35. Fracture surface of coupling 44.

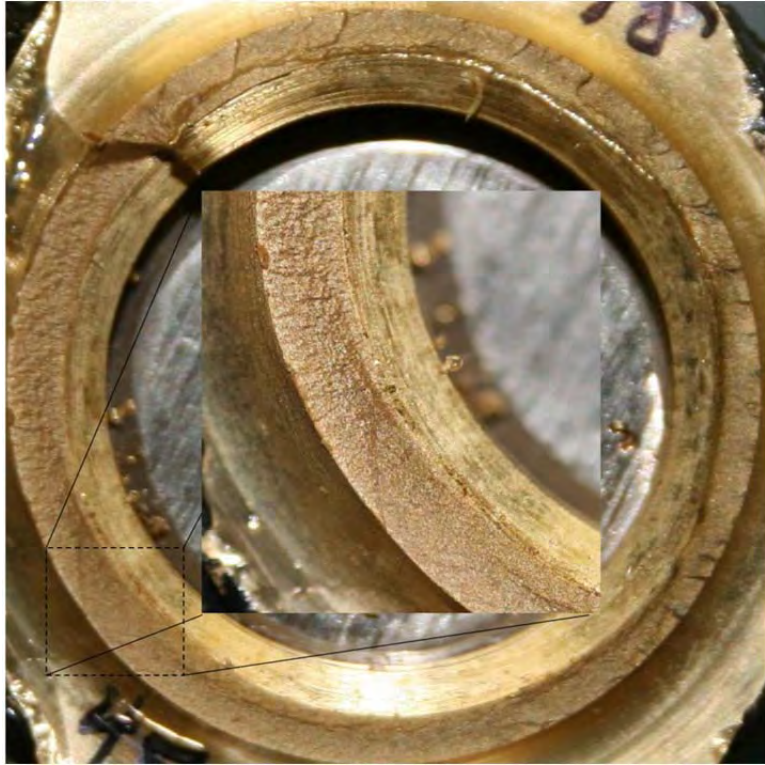


Figure 36. Fracture surface of coupling 45.

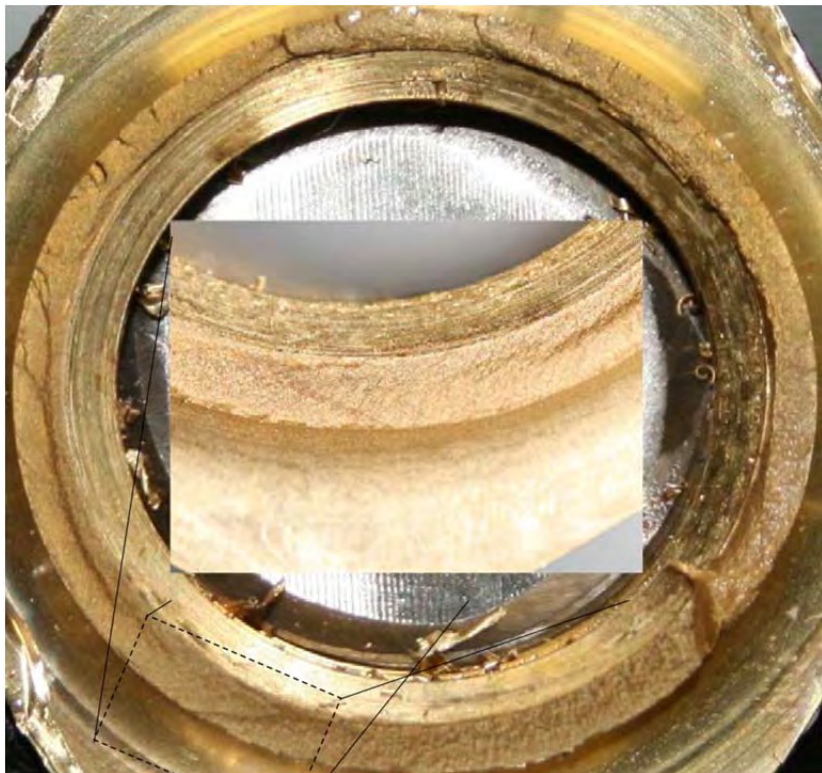


Figure 37. Fracture surface of coupling 46.



Figure 38. Fracture surface of coupling 51 (failed in tension).



Figure 39. Fracture surface of coupling 52.



Figure 40. Fracture surface of coupling 53.



Figure 41. Fracture surface of coupling 54.

## CHAPTER 5 FINITE ELEMENT ANALYSIS

The purpose of finite element analysis (FEA) in this study was also used to calculate the stress concentration factor,  $K_t$ , for circular members with internal and external notches in tension and compression to compare it with strain gaging or the loading of plastic models which generate interference patterns. The finite element method is particularly useful for items of limited size or complexity where strain gages cannot be mounted to determine stress concentrations or the similarity of modeling is imprecise.

A simplified, two-dimensional model was selected (Figure 42), which served to calculate  $K_t$ . The FEA model was verified by using the experimental data generated earlier. Finite element modeling was performed with ABAQUS® using an isotropic planar model. The mechanical properties of CDA 360 brass previously determined by monotonic tensile testing of specimens were used as the material characteristics for the FEA model. Only the linear response of the coupling model was considered because of the low stress range of the couplings. It is expected that the CDA 360 brass couplings will remain in the linear elastic portion of the stress vs. strain curve during actual service.

Multiple element sizes were considered, with smaller elements giving results closer to experimental values. The two-dimensional model results showed an approximate agreement with experimental data when the number of element edge length was set to 0.0001 in. or less. Due to the required small element size, much higher computing power was required to run the model, so only a minimal section of the coupling was considered. The central 0.500 in. of the coupling was accurately modeled in two dimensions to maximize element density with respect to maximum element size with the given computing limitations (Figure 43). Using only the central 0.500 in. of the coupling and an element edge length of 0.0001 in., a mesh was created using the sweeping front option in ABAQUS®, resulting in a total number of 143,321 elements (Figure 44).

The loading condition that produced results most similar to experimental measurements was a uniform loading applied to the top and bottom edges of the model (Figure 43). ABAQUS Viewer® was used to extract maximum in-plane stresses of selected elements. The stress concentration for internal notches was 13.1, and 12.8 for the external notches. Both of the stress concentration factors determined by FEA were higher than those observed by experimental measurements. The stress concentrations produced by the model were most probably influenced by the element density and whether loading conditions are truly accurate. A two-dimensional model of only the center section also did not completely capture the realistic boundary conditions of the coupling. However, FEA determination of stress concentration factors of internal and external notches was shown to be comparable with strain gage and theoretical methods within 20 to 30% accuracy.



Figure 42. Two-dimensional cross section.



Figure 43. Minimal section analyzed with loading conditions.

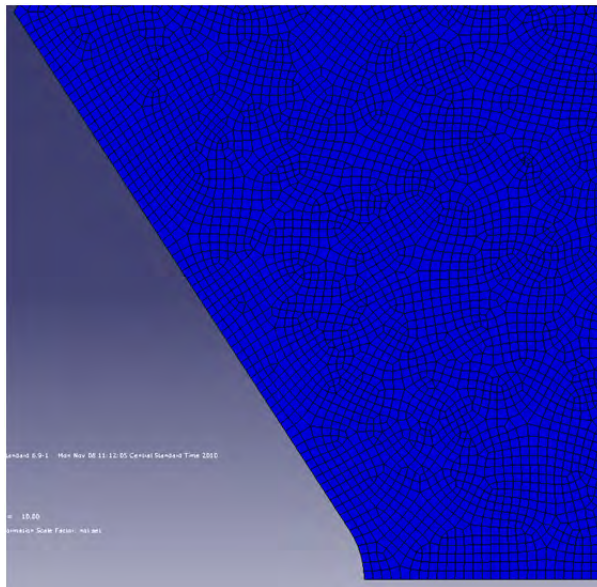


Figure 44. Representative element density of the finite element model.

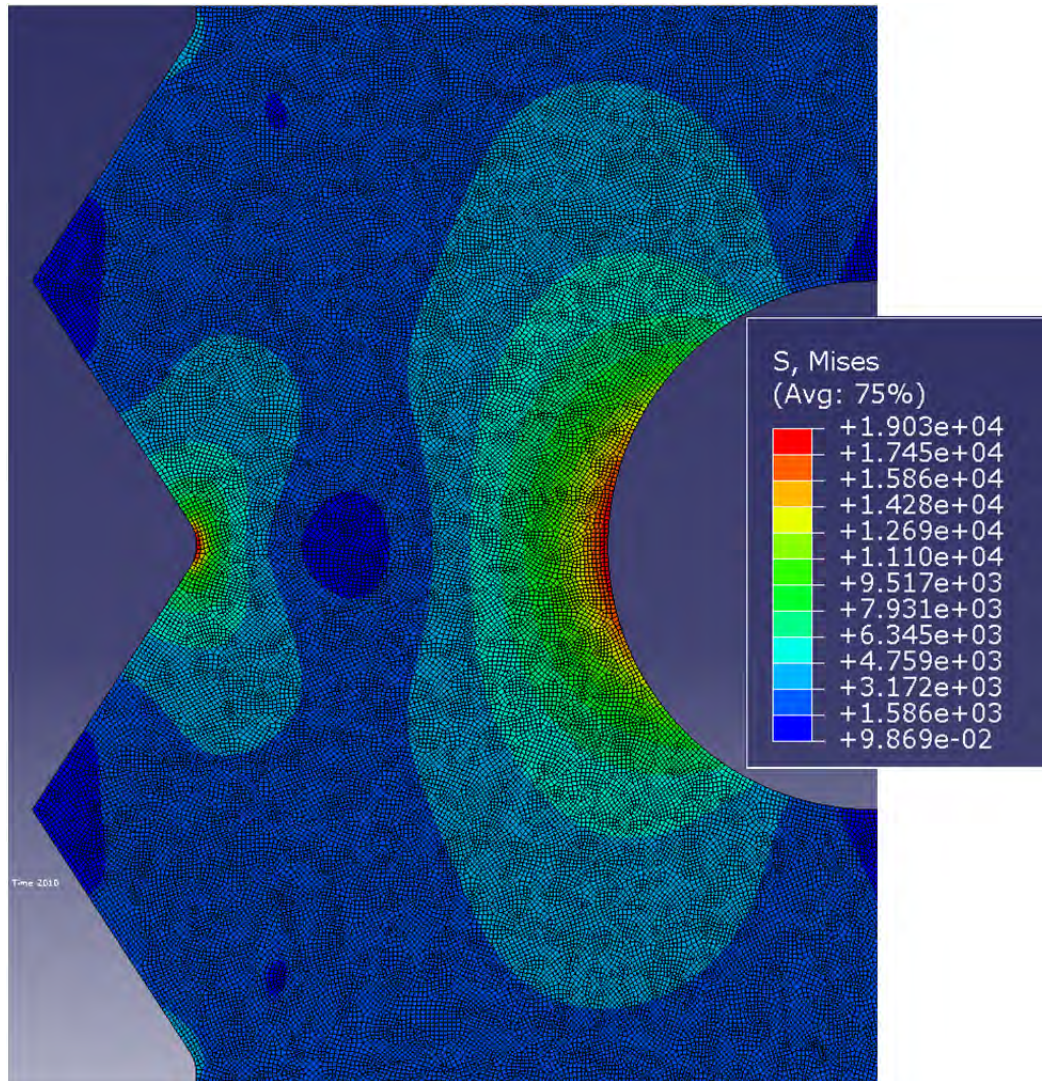


Figure 45. Finite element stress ranges of critical notches.

## CHAPTER 6 EFFECTS OF WIND LOADS ON COUPLINGS

Light poles and other tall structures are subjected to wind loads that vary with wind speed and direction. Light poles generally use tapered hollow tubes to support a luminaire. The tapered aluminum alloy or steel tubes are typically fillet-welded to a thick base plate. A typical base plate usually has four holes that connect the couplings to the base plate and the anchor bolts. The pole acts as a cantilever subject to variable moments applied as a result of changes in wind pressure along its length due to tapering of the cylinder and different drag coefficients. These individual moments, when combined, result in tensile and compressive stresses applied to the four couplings that are repeated as a function of the fundamental frequency of oscillation of the pole.

The occurrence of 80 mph winds appears about every 50 years in Illinois. There have been no reported occurrences of sustained 90 mph winds in Illinois (AASHTO 1985). Winds of 90 to 100 mph are common along the Atlantic coastal areas of the United States and along the Pacific coastal states of Oregon and Washington (AASHTO 1985).

The average wind speed in major Illinois cities ranges from 9.7 to 10.9 mph (NOAA 2011). Typical high speed winds in Illinois range from 60 to 70 mph, based on a 25 year mean recurrence interval (AASHTO 1985). Because wind pressure is a squared function of velocity, speeds of 60 to 70 mph have substantially less wind pressure compared with wind speeds at 90 mph. Wind pressures at 60 mph are only 44% of the pressures at 90 mph; at 50 mph, they are only 31%.

The calculation of wind forces on a light pole can be very detailed, but one can use the more simplified method recommended in the AASHTO *Standard Specifications for Structural Supports for Highway Signs, Luminaires and Traffic Signals* described in the appendix (AASHTO 1985). The following analysis is a more detailed method that takes into account that height and drag coefficients vary as a function of pole diameter, wind speed, and height above ground level. The example calculation is for a 40 ft steel light pole, commonly used in Illinois, which has a circular section, a base diameter of 10 in. and a 4 in. diameter at the top. These poles have a linear taper of 0.15 in/ft. Because luminaire designs, sizes, and arm lengths substantially vary, they were not taken into account in this analysis.

For safety purposes, AASHTO requires that light poles must be able to withstand 90 mph winds. The attachment of breakaway couplings to a pole is a balancing act that permits rupture upon vehicular impact yet still provides an adequate fatigue life of the pole during a severe wind storm. CDA 360 free-cutting brass has a nearly constant Charpy V-notch toughness at 14 ft-lb from  $-20^{\circ}\text{F}$  to  $+80^{\circ}\text{F}$  and has good long-term fatigue life in the half-hard condition. In the following analysis, stresses and fatigue life were calculated for wind speeds on poles ranging from 40 mph to 90 mph. Emphasis was placed on 90 mph because it is the maximum required condition by AASHTO for acceptance.

Wind pressures are conventionally determined by the exposed projected area of a pole or segments of a pole. These pressures are modified by the shape and diameter of the pole and the variation in wind speed as function of height. This analysis breaks down the pole into four 10 ft long segments and takes the median diameter of each segment. Each segment contributes an individual moment, all of which are then added up to provide a combined total moment. The total moment is used to calculate the resulting stresses applied to the breakaway couplings.

Wind pressure,  $P$ , as shown in the following equation (AASHTO 1985), is expressed in customary units of  $\text{lb}/\text{ft}^2$ :

$$P = 0.00256 V^2 \times C_d \times C_h$$

where

$V$  = wind speed, mph

$C_d$  = drag coefficient

$C_h$  = height coefficient

The dominant part of the wind pressure equation is  $V^2$ , where the speed of the wind exponentially increases pressure. The drag coefficient,  $C_d$ , is an inverse exponential function (AASHTO 1985), which is determined by the following equation:

$$C_d = 100 \div [Vd]^{1.3}$$

where

$V$  = wind speed, mph

$d$  = diameter of round pole, ft

When the product,  $Vd$ , is less than 32,  $C_d$  is held constant at 1.1; if  $Vd$  is greater than 64, it is held constant at 0.45. Because the drag coefficient changes with diameter and wind speed, it results in considerable variations of pressure as a function of pole height. The drag coefficient is an inverse function, whereby drag increases with height because pole diameter decreases with height. Drag coefficients as function of the height of a 40 ft tapered pole at 90 mph are shown in Figure 46.

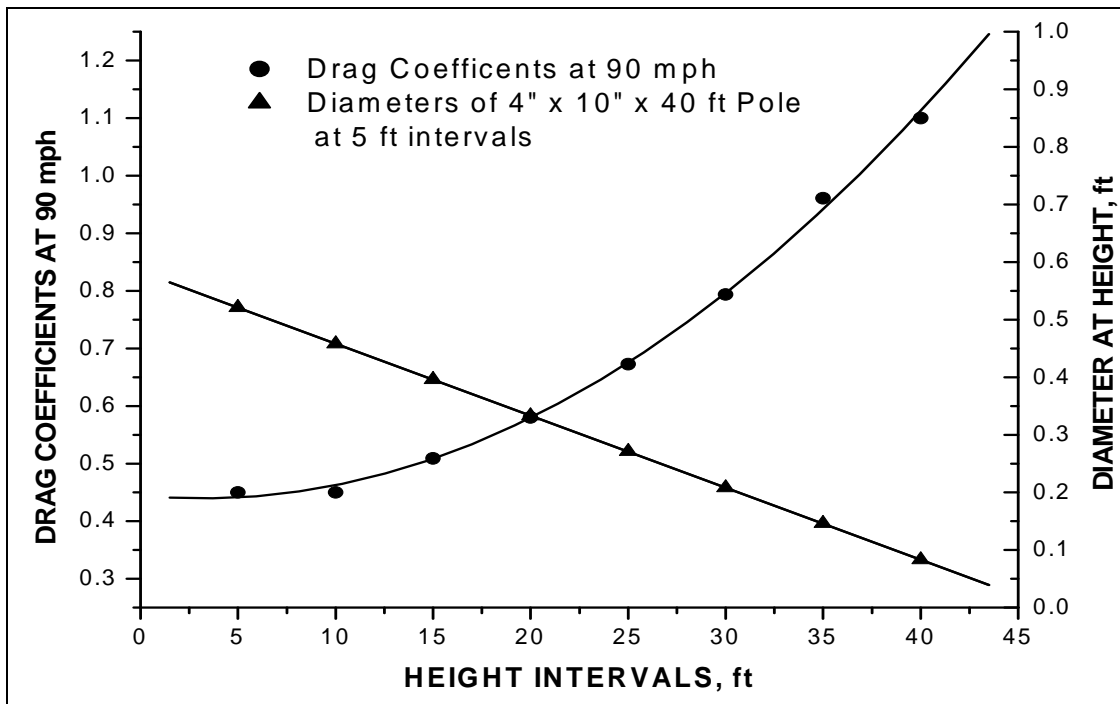


Figure 46. Drag coefficients at various pole heights and respective diameters for a 40 ft tapered pole with a 10 in. base and 4 in. at the top, at a 90 mph wind speed.

The height coefficient is a weaker exponential function compared with the drag coefficient and is based on a reference value of 1.00 at 33 ft:

$$C_h = [Z \div 33]^{0.28}$$

where  $Z$  = height, ft

This equation is taken from the *Structural Engineering Handbook* (Chang et al. 1997). The exponent 0.28 of the height function has been verified by independent modeling studies shown to be quite accurate (Shiau and Chang 2008). Ground conditions, such as the presence or absence of trees, structures, or other obstacles, substantially alter wind speed as a function of height. The effect of height from 5 to 40 ft for open conditions without tree cover on wind pressure is shown in Figure 47.

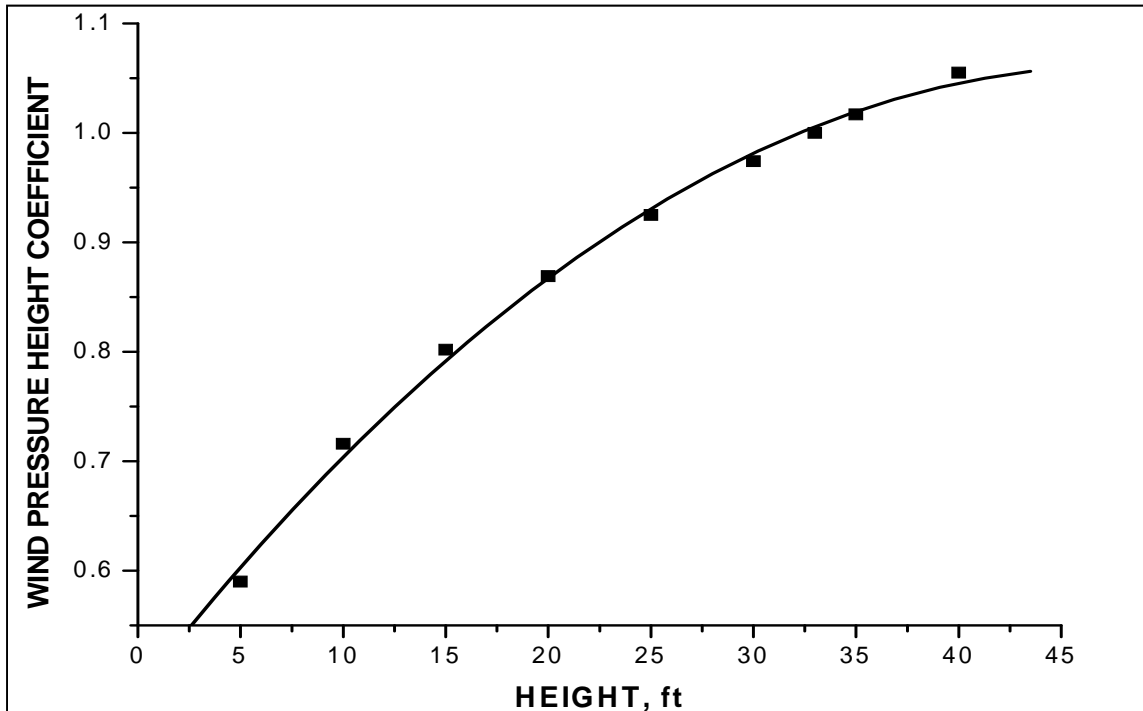


Figure 47. Height coefficients for a light pole at 5 ft intervals, based on the equation  $C_h = [Z / 33]^{0.28}$ .

In this segmental approach to determination of wind pressure as a function of diameter and height, the pole is divided into four 10 ft sections, starting at the bottom diameter at 10 in. and progressively moving upward to the top at 4 in. diameter. Each 10 ft segment has a frontal projected area, and the mean diameter is taken at the midpoint. The projected area of each segment is  $A = \frac{1}{2} (a + b) \times h$ , where  $a$  is the diameter at the bottom of each 10 ft long segment,  $b$  is the diameter at the top, and  $h$  is the height (fixed at 10 ft). Each 10 ft segment has a different drag coefficient and height coefficient. The wind pressure at a specific wind speed remains the same at  $P = 0.00256 V^2$ , but the actual forces on each segment vary because the drag and height coefficients change.

Each 10 ft segment exerts a moment on the base of the pole, based on the force generated from the wind pressure and the distance from the base of the pole. These moments are:

$$M_t = P_1 \times d_1 + P_2 \times d_2 + P_3 \times d_3 + P_4 \times d_4$$

where

$M_t$  = total of individual moments

$$P_i = 0.00256V^2 \times A_i$$

$d_i$  = distance from base to center of each 10 ft segment

$A_i$  = projected frontal area of each segment

As calculated in the appendix of this report, the moment of inertia for the couplings in the diamond and square configurations is the same at 220 in<sup>4</sup>. The diamond configuration is where two couplings are aligned within the neutral axis, and the wind direction is perpendicular to the neutral axis. The coupling facing the wind is in tension; the coupling on the leeward side is in compression. For the square configuration, the neutral axis passes exactly between the four couplings, the wind direction is perpendicular to the neutral axis, and two couplings directly face the wind. The square configuration places two couplings facing the wind in tension, with the other two couplings on the leeward side in compression when the pole cantilever is subject to moment action. The drag and height coefficients for mean diameters for each 10 ft segment, the forces induced by wind pressure, and the individual moments for a tapered 40 ft pole subjected to 90 mph winds, are summarized in Table 10.

Table 10. Summary of Drag and Height Coefficients, Diameters, Forces and Moments

Segment*	Drag Coefficient	Height Coefficient	Diameter*, ft	Area of Segment, ft <sup>2</sup>	Segment Wind Force, lb	Moment, in.-lb
0 to 10 ft	0.450	0.590	0.770	7.705	42.45	2,547
10 to 20 ft	0.509	0.802	0.646	6.455	54.61	9,830
20 to 30 ft	0.673	0.925	0.521	5.205	67.20	20,160
30 to 40 ft	0.961	1.017	0.396	3.955	80.17	33,671

\*The diameter is taken at the midpoint of each 10 ft segment (at 5, 15, 25, and 35 ft, respectively).

At 90 mph, the total combined moment applied to the pole at 90 mph is 66,208 in.-lb. The diamond configuration exerts the greatest stress on a coupling because its radius is 7.5 in. compared with 5.3 in. for the square configuration. The nominal stress is calculated conventionally:

$$\sigma_n = [M_t \times R] \div I$$

where

$\sigma_n$  = nominal stress, psi

$M_t$  = combined moments from all four segments

R = radius of the coupling array

I = moment of inertia of the four couplings

The resulting nominal stress is 2,257 psi in the hexagon portion of the couplings. However, the stress concentration,  $K_t$ , in direct tension is between 10.4 in compression and 10.8 in tension. Using a  $K_{t,avg}$  average of 10.6, this causes a peak stress in the notched coupling to be 23,924 psi.

Because poles oscillate during a windstorm, this generates an alternating stress of compression-to-tension  $\Delta S$  in the notch, where  $\Delta S = 23,394 \times 2 = 47,848 \text{ psi} \approx 47.9 \text{ ksi}$ . The cyclic fatigue testing performed at the University of Illinois provided a high cycle tension-compression fatigue relationship,  $\Delta S = 433 \times N^{-0.153}$ . In the case where the wind speed is 90 mph,  $\Delta S = 47.9 \text{ ksi}$  for the worst-case (diamond) configuration. To calculate N, the number of cycles to failure, the equation is placed in logarithmic form:

$$\log 47.9 = \log 433 - 0.153 \log N$$

$$-0.153 \log N = -0.957$$

$$\log N = 6.255$$

$$\text{therefore, } N = 1.799 \times 10^6 \text{ cycles}$$

This result does not take into account the weight of a light pole, which would decrease the tensile forces that induce the most fatigue damage. Aluminum poles would have about one-third the weight of a comparable steel pole.

The amount of fatigue life was calculated in terms of millions of cycles for wind speeds from 40 mph up to 90 mph. The amount of fatigue damage greatly decreases at 50 mph. The fatigue life of brass couplings for tapered 40 ft light poles at wind speeds varying from 40 mph up to 90 mph is summarized in Table 11, which clearly indicates that the couplings have sufficient fatigue life at the highest wind speeds (80 to 90 mph) recorded in Illinois.

Table 11. Summary of Peak Concentrated Stresses at Various Wind Speeds

Wind Speed, mph	Peak Tensile Stress, psi*	Fatigue Life, millions of cycles
40	7,060	5,235
50	10,865	450
60	14,776	41
70	18,200	11
80	21,730	3.2
90	23,924	1.8

\*This is the concentrated stress at the coupling notch, which has a  $K_{tavg}$  of 10.6 when the brass couplings are in the diamond configuration where the neutral axis passes through the center lines of two couplings.

## CHAPTER 7 BENDING STRESSES AND FATIGUE LIFE

Because CDA brass is a very ductile copper alloy, the “bending stresses” may plastically redistribute the localized strain, resulting in an aggregate net stress spread over a wider area. This phenomenon, which is seen in the crack initiation sites in Figures 25 through 37, does not always start at a specific defined point but more often originates from a narrow zone of crack initiation of 20° to 35° of the circumferential area between the ID and OD of the notched portion of the coupling. In contrast, for metals with limited ductility of 2% or less, such as spring wire, the initiation sites can be very confined and easily discerned.

Table 6 (see Section 4.3 of this report) compared the differences in wall thickness for seven different couplings at various points. Although wall thicknesses vary by 1.9% to as much as 9.0%, the stress concentration factor of  $K_t = 10$  magnifies these stresses so that they result in greater strain at one point compared with another when axially loaded, resulting in areas of net tension and net compression. Hence, the references to “bending stresses” used in this report are for the axial tests.

When individual couplings of Design 1 were loaded in bending, they showed significantly higher differences in strain between the nominal and reduced sections than when loaded in a light pole base configuration. A stress concentration factor of  $K_t = 5.7$  was determined from couplings of Design 1 when loaded individually in bending. Design 1 showed a very low sensitivity to applied stress range to fatigue life. Bending testing of Design 2 showed a higher stress concentration factor of  $K_t = 9.0$  compared with Design 1 because of the deeper notch cut. The fatigue life of Design 2 was more sensitive to the applied stress level, principally from the eccentricity effects of drilling and tapping, the increased notch depth, and decreased wall thickness of the notched area. Taking notch depth and acuity into account, 23.9 ksi is the peak stress generated at 90 mph wind speed previously determined by the detailed segmental method. When bending is taken into account, the peak stress is 38 ksi, which is 84% of the typical yield strength for CDA 360 brass. When installed by applying the proper torque of 50 to 75 ft-lb, with minimal differences in the wall thickness of the notched area due to precise drilling and tapping, the couplings are predicted to have a cyclic life of  $10^6$  cycles at a wind speed of 90 mph for Design 1 with no rain, snow, or ice loading. When additional ice and snow loading is included, the increased mass of the pole induces compressive forces in the couplings, which would increase fatigue life. At present, there are no provisions in AASHTO standards to account for rain load, but the AASHTO gust factors of 30% could provide a rough approximation (AASHTO 1985).

In the appendix, sample calculations using the simplified method of AASHTO Standards (1985) are presented to determine stresses in the couplings for poles subjected to 90 mph winds. If the stress concentration factor  $K_t = 7.15$ , the stress in the coupling is 15,940 psi. If  $K_t = 10.8$ , the notch stress is 24,080 psi, then the completely reversed stress range is 48,160 psi. As shown in to Figure 24, the couplings at 24,080 psi with complete reversal would have an estimated 1,693,000 cycles of life at a 90 mph wind speed.

Stress concentration factors were developed based on a perfectly symmetrical notch with uniform wall thickness. However, if there are deviations from the uniformity of the wall thickness at the notch caused by eccentric drilling and tapping, stresses can increase in the areas of least thickness, further increasing stress levels already concentrated by the notch geometry itself, leading to crack initiation. In the diamond configuration, peak stresses induced by bending were at or near yield at 38 ksi at  $K_t = 10.8$ . At this stress level, complete reversal results in a stress range of  $\Delta S = 76$  ksi (+38 ksi in tension; -38 ksi in compression). Using the relationship  $\Delta S = 433 N^{0.153}$ , fatigue life at the 38 ksi alternating stress level is estimated to be only 86,270 cycles (50% mean). However, calculated stresses based on

wind pressures result in a peak stress of 26.9 ksi, where fatigue life is estimated at 825,000 cycles, using the same fatigue life equation. A storm with 85 to 90 mph winds, a very rare occurrence in Illinois, would be of short duration, typically less than 30 minutes. Because the fundamental frequency of most steel poles is about 1 Hz (1 cycle/sec), 1800 cycles are sustained in 30 minutes. This number of cycles is about 2% of the available life at the 38 ksi alternating stress level and is only 0.2% of life at an alternating stress of 26.9 ksi for a steel pole.

The use of single specimens for fatigue testing gives the impression of a limited fatigue life in actual service. However, this impression is misleading because it does not consider other factors that extend life in actual service. Although the wall thickness of the notch varies on average by 4.2% up to a maximum of 9.1%, the probability that all couplings will have their weakest orientation perfectly aligned to provide easy failure is very small. If approximately 30° is the susceptible fatigue zone, the probability that it aligns with a high-speed wind direction is about 30°/360°. The probability that all four couplings will be perfectly aligned will be even smaller at 30°/360°/4 = 0.021, or about 2.1% of the time. The greatest deviation in notch wall thickness was 9%. Permitting a 9% increase in notch wall thickness will take into account straightness tolerances in brass hexagon starting stock and any small machine chucking deviations.

Finally, when the mass of steel or aluminum poles is included, anticipated tensile stresses can be decreased than those in the simplified calculations shown in the appendix. At a peak stress of 38 ksi, tensile stresses are reduced by the weight of the pole. A 40 ft aluminum pole with a 10 in. base and 4 in. top and a 0.25 in wall thickness weighs 210 lb. A 40 ft steel pole of the same dimensions with a 7 gage (0.1793 in.) wall thickness weighs 265 lb. Because of the compressive stresses induced by the weight of the light pole and the stress concentration factor of 10.4, a stress of -2,283 psi develops in the notch. The 38 ksi peak tensile stress would be decreased by (38 ksi - 2.3 ksi) = 35.7 ksi. Increasing compressive stress, accompanied by a decrease in tensile stress, results in a decrease of mean stress. Mean stress is defined by the relationship:

$$\sigma_m = [S_{max} + S_{min}] / 2$$

In this case, after the pole weight is taken into account,  $S_{max} = 35.7$  ksi and  $S_{min} = -40.3$  ksi, resulting in a mean stress of -2.3 ksi. When the mean stress is compressive, fatigue life increases and crack propagation rates decrease for steel and aluminum alloys because the tensile stresses are the most damaging. The beneficial effects of mean compressive stress have been authenticated by many fatigue studies (Fuchs and Stephens 1980; Collins 1981) and can be accounted for (Hertzberg 1989) by use of the Goodman relationship:

$$\sigma_a = \sigma_{ftg} [ 1 - (\sigma_m / \sigma_{ts} ) ]$$

where

$\sigma_a$  = alternating stress when  $\sigma_m$  is not 0

$\sigma_{ftg}$  = fatigue strength when  $\sigma_m = 0$ ; 20 ksi at  $10^8$  cycles for rotating beam

$\sigma_m$  = mean stress, -2.3 ksi

$\sigma_{ts}$  = tensile strength, 55 ksi for CDA 360

In the case considered where  $\sigma_{ftg} = 20$  ksi, the new  $\sigma_a = 21$  ksi permitted the coupling to sustain slightly higher alternating stress levels by about 4% above the fatigue strength in

rotating bending at zero mean stress without fatigue failure. As the weight of the light pole increases, the greater the compressive stresses introduced into the coupling notch.

Assuming that the slight increase in compressive stresses do not provide any life extension, at 38 ksi alternating stress, the reversed stress range of  $\Delta S = 76$  ksi, where the number of stress cycles was previously calculated at a 50% mean life of 86,270 cycles. For a windstorm of 30 minutes duration at 90 mph, which is beyond the limit of recorded occurrences in Illinois, the pole would sustain this wind speed for 1800 seconds. The typical fundamental frequency for steel light poles is about 1 Hz, whereby 1800 cycles of alternating stress at 38 ksi would consume only 2% of available coupling fatigue life.

Calculated stresses based on known wind pressure equations, using more accurate segmental methods, predicted a peak stress of 26.9 ksi, whereby tensile stresses would be further reduced by  $-1.8$  ksi for a 210 lb aluminum pole and  $-2.3$  ksi for a 265 lb steel pole, thereby providing a slight increase in available life. Even if compressive stresses are not included, a stress range of  $+26.9$  ksi to  $-26.9$  ksi results in a significantly increased life of 822,304 cycles at the 50% mean of the data scatter.

## CHAPTER 8 CONCLUSIONS

Testing of the first design of couplings was performed by loading a steel tube attached to a base plate bolted to a concrete base, which was then attached to a specially made steel plate and tube fastened attached to the strong wall of the Newmark Structural Engineering Laboratory at the University of Illinois. When alternating loads were applied, this placed the couplings in a bending mode. Bending testing showed that exact planar placement of the couplings can be difficult to achieve and that deviations from perfect symmetry can result in a definitely non-linear stress response of the couplings. Loading of individual couplings showed linear, repeatable results, whereas the “diamond” and “square” configurations of base plates under load showed initial non-linear, non-repeatable behavior at lower stress levels, but they became linear after loadings increased. Stresses in opposing couplings, however, did not have perfectly equal compression-tension symmetry as predicted by structural theory. The variable behavior of the resulting stresses in the “square” and “diamond” configurations showed that small changes in the testing setup can have significant effects on the induced stresses, which were caused by eccentricities in the testing setup, as well as drilling and tapping of the couplings and variances in the concrete base. The setup for the bending testing was less rigid than that used for other testing performed for this project. Although the bending testing did not achieve ideal agreement with theoretical calculations, it may be very comparable to what is achievable in field installations of the couplings.

Fatigue testing was performed on the first design. Because of the eccentricity of the center hole of the coupling and possible eccentricities of the testing frame, significant levels of bending stress developed when specimens were axially loaded. The bending stresses were not noticed until the fatigue testing of the fifth coupling, at which point more strain gages were applied to measure the severity of the bending stresses. A significant amount of data scatter was noted when the bending stresses were measured. No direct connection was discerned between the levels of bending stresses recorded compared with any specific testing variable.

Additional designs of couplings were presented for testing by IL DOT. The second and third designs were abandoned within one month after receiving them, and a fourth design was chosen as the final design for tension and impact testing. One coupling each of the second and third coupling designs was tested in fatigue; however, additional specimens are required for further analysis.

The fourth design was tested in bending using only a single coupling, allowing the use of a more rigid testing setup. An additional hole was drilled in an existing angle plate, and the plate was attached to a rigid testing frame. The revised design of the notch decreased the radius of the external notch by 1/16 in. and removed the bevel on each side of the notch, which did not allow for the placement of strain gages, so an extensometer was used instead. Using the more rigid testing frame, expected and repeatable results were obtained.

Fatigue testing of the fourth design was performed in the same testing setup as for the other designs. Each coupling had three gages placed 120° degrees apart to measure bending stresses. Because of time constraints, stress levels were increased to reduce the fatigue lives; , therefore, the ranges of fatigue lives did not overlap with previous testing. Bending stresses ranged from 15% to 78% of the applied axial stresses, with an average of 37%. Using the bending stresses led to an even larger scatter than was evident in the first design. When bending stresses were removed from the results, the scatter of the fatigue data were significantly reduced, possibly indicating that plastic deformation was occurring at the higher stress levels applied.

Finite element modeling results were similar to those achieved by experimental testing. The stress concentration factor determined from the minimal two-dimensional section was within 20% of the  $K_t$  that was experimentally determined. The two-dimensional model was useful in helping to determine the stress concentration of a member with internal and external notches.

AASHTO standard structural theory (1985) was used to determine the average stress in each coupling of 40 ft poles subjected to winds at 90 mph, and was calculated at 24.1 ksi, taking a stress concentration factor of  $K_t = 10.8$  into account. Using a more refined segmental method, and taking an average of the stress concentrations determined in tension and compression at  $K_{t,avg} = 10.6$ , the peak tensile stress was calculated at 23.9 ksi. For a completely reversed stress range of 47.8 ksi, and using the fatigue relationship of  $\Delta S = 433 N^{-0.153}$  determined by reversed tension-compression tests, the notched brass couplings of Design 4 would have a 50% mean stress life of 1,789,000 cycles.

When bending stresses, caused by variations in the notch zone wall thickness, were taken into account, the peak stress generated was  $23.9 \text{ ksi} \times 1.37 = 32.7 \text{ ksi}$ . This peak stress was 73% of the minimum yield strength of half-hard CDA 360 brass. The stress range would be 65.4 ksi, reducing fatigue life to 230,270 cycles. However, compressive stresses from the weight of the pole slightly reduce this stress by about  $-1.8 \text{ ksi}$  for a 40 ft aluminum pole at 210 lb, and  $-2.3 \text{ ksi}$  for a 40 ft steel pole at 265 lb. Compressive stresses reduce the mean stress, depending on the weight of the pole, permitting the coupling to operate at slightly higher alternating stresses. The compensation for mean stress would increase the allowable alternating stress. This decreases the likelihood of failure, as shown by use of the Goodman failure criteria, as shown in the previous chapter.

For a 90 mph windstorm of 30 minutes duration, which is just beyond the limit of recorded occurrences in Illinois, and a stress range of  $\Delta S = 65.4 \text{ ksi}$ , the pole would sustain 1800 cycles. For many steel light poles, whose typical fundamental frequency is 1 Hz, a total of 1800 cycles of alternating stress out of 230,270 available cycles would consume only 0.8% of coupling fatigue life.

The statistical probability of having each coupling being exactly positioned in the weakest orientation was estimated to be about 2%. With the occurrence of 90 mph winds occurring about every 50 to 75 years in Illinois, the brass breakaway couplings should have a long fatigue life because they also have a higher atmospheric corrosion resistance compared with steel couplings.

## CHAPTER 9 FURTHER STUDY

The effect of bending stresses on the reduced section may be more complex than first envisioned. The theoretical stress concentration factors proposed by Peterson (1974) are significantly lower than those observed in the current study, indicating either a possible interaction of the internal threads and external surfaces or an artifact of the bending stresses.

To find a definitive answer, further experimental work is recommended to study the effects of bending and thread root stresses more thoroughly and verify the results of the finite element analysis. With several data points for applied stresses and respective fatigue life, results from finite element modeling can be factored in appropriately, and fatigue behavior over a broader range of bending and applied stresses could then be estimated. However, physical testing should be performed to verify the finite element models. The finite element analysis performed in this study could not sufficiently model the realistic loading behavior because of the minimized height analyzed and the two-dimensional boundary conditions. The effect of differing notch geometry is also a concern because the two designs tested have different cross-sections and notch acuity. The beveled notch of the first design was also removed in favor of a circular and sharper notch, which would have some effect on the stress concentration factor. While this effect was assumed not to be significant in this study, experimental testing may show a significant difference.

Further study should also include measuring the effect of variable side wall dimensions at the notch on fatigue life by comparing a drilled and tapped specimen from a hollow brass round instead of a hexagon. The round would be machined by turning to make its central axis of the chuck collinear with central axis of the threaded hole. This minimizes the extent of eccentricity associated with a cold-drawn brass hexagon which is not always perfectly straight. The fatigue results from turned, hollow threaded cylinders would then be compared with couplings machined from hexagons as described in this report. This comparison will determine whether the inherent data scatter is from the internal threads, their inclusions, and surface roughness, or if they are predominantly from additional bending stresses as a result of variable wall thickness originating from drilling and tapping operations.

## REFERENCES

- Akyildiz, H. K., and Livatyali, H. 2010. "Effects of Machining Parameters on Fatigue Behavior of Machined Threaded Specimens." *Materials and Design* 31:1015-1022.
- Aryassov, G., and Petritshenko, A. 2008. "Analysis of Stress Distribution in Roots of Bolt Threads." *Proceedings of the 19th International DAAAM Symposium*, pp. 35-36.
- American Association of State Highway and Transportation Officials (AASHTO). 1985. *Standard Specifications for Structural Supports for Highway Signs, Luminaires and Traffic Signals*, pp. 9-19. Washington, DC: AASHTO.
- ASTM. 2005. *Standard Practice for Verification of Test Frame and Specimen Alignment Under Tensile and Compressive Axial Force*. ASTM Standard E1012. West Conshohocken, PA: ASTM.
- ASTM. 2010. *Standard Specification for Free-Cutting Brass Rod, Bar and Shapes for Use in Screw Machines*. ASTM B16. West Conshohocken, PA: ASTM.
- Azzam, D., and Menzemer, C. C. 2006a. "Fatigue Behavior of Welded Aluminum Light Pole Support Details." *Journal of Structural Engineering* 132(12):1919-1927.
- Azzam, D., and Menzemer, C. C. 2006b. "Residual Stress Measurement of Welded Aluminum Light Pole Supports." *Journal of Structural Engineering* 132(10):1603-1610.
- Berger, C., Pyttel, B., and Trossmann, T. 2006. "Very High Cycle Fatigue Tests with Smooth and Notched Specimens and Screws Made of Light Metal Alloys." *International Journal of Fatigue* 28:1640-1646.
- Carlyle, A. G., and Dodds, R. H. 2007. "Three-Dimensional Effects on Fatigue Crack Closure under Fully-Reversed Loading." *Engineering Fracture Mechanics* 74:457-466.
- Chu, S., Fang, S., and Zar, M. 1997. "Chimneys," pp. 32-33. In *Structural Engineering Handbook* (4th ed.) Edited by Gaylord, E.H., Gaylord, C.N., and Stallmeyer, J. E. New York: McGraw-Hill.
- Collins, J. A. 1981. *Failure of Materials in Mechanical Design*, pp. 214-234. New York: Wiley-Interscience.
- Crawford, R. J. 1974. "A Comparison of Uniaxial and Rotating Bending Fatigue Tests on an Acetyl Co-Polymer." *Journal of Materials Science* 9(8):1297-304.
- Elmarakbi, A., Sennah, K., Samaan, M., and Siriya, P. 2006. "Crashworthiness of Motor Vehicle and Traffic Light Pole in Frontal Collisions." *Journal of Transportation Engineering* 132(9):722-734.
- Fuchs, H. O., and Stephens, R. I. 1980. *Metal Fatigue in Engineering*, pp. 69-76. New York: Wiley.
- Fukuoka, T., and Nomura, M. 2008. "Proposition of Helical Thread Modeling with Accurate Geometry and Finite Element Analysis." *Journal of Pressure Vessel Technology* 130(1).
- Fukuoka, T., and Takaki, T. 2003. "Elastic Plastic Finite Element Analysis of Bolted Joint During Tightening Process." *Journal of Mechanical Design* 125:823-830.

- Grover, H. J., Gordon, S. A., and Jackson, L. R. 1960 (June). "Fatigue of Metals and Structures". NAVWEPS Report 00-25-534. Washington, DC: Department of the Navy.
- Hertzberg, R. A. 1989. *Deformation and Fracture Mechanics of Engineering Materials* (3rd ed.), pp. 466-467. New York: Wiley.
- McAdam, D. J. 1925. "Endurance Properties of the Alloys of Nickel and Copper." *American Society of Steel Treating Transactions* 8:54-81.
- Mnif, R., Elleuch, R., and Halouani, F. 2010. "Effects of Cyclic Torsional Prestraining and Overstrain on Fatigue Life and Damage Behavior of Brass Alloy." *Materials and Design* 31:3742-3747.
- Moore, H. F., and Lewis, R. E. 1931. "Fatigue Tests in Shear of Three Non-Ferrous Metals." *ASTM Proceedings* 37:236-242.
- National Oceanic and Atmospheric Administration (NOAA). 2011. "Recorded Average Wind Speed Data through 2001 in Illinois." NOAA Website.
- Ong, J. H. 1933. "An Improved Technique for the Prediction of Axial Fatigue Life from Tensile Data." *International Journal of Fatigue* 15(3):213-219.
- Peterson, R. E. 1974. *Stress Concentration Factors*, p. 70. New York: Wiley.
- Shiau, B., and Chang, H. 2008. "Measurements on the Surface Wind Pressure Characteristics of Two Square Buildings Under Different Wind Attack Angles and Gaps," p. 3. Bluff Bodies Aerodynamics and Applications Colloquium, Milan, Italy, 20-24 July 2008.
- Stoughton, R. L., Abghari, A., Dusel, J. P., Hedgecock, J. L., and Glauz, D. L. 1989. "Vehicle Impact Testing of Lightweight Lighting Standards." *Transportation Research Record* 1233:51-64.
- Tanaka, M., Miyazawa, H., Asaba, E., and Hongo, K. 1981. "Application of the Finite Element Method to Bolt-Nut Joints—Fundamental Studies on Analysis of Bolt-Nut Joints Using the Finite Element Method." *Bulletin of the JSME* 24(192):192-223.
- Transpo Industries Inc. No date. "Pole-Safe® Omni-Directional Breakaway Pole Support Systems from Transpo." New Technology for Transportation Safety from Transpo Industries, Inc. <http://www.transpo.com/pole-safe1.htm> (accessed 16 August 2010).
- Tyler, D. E. 1990. "Properties of Wrought Copper and Copper Alloys," pp. 310-311. In *ASM Metals Handbook, Vol. 2, Properties and Selection, Non-Ferrous Alloys and Special Materials*. Materials Park, OH: ASM International.
- Walton, N. E., Hirsch, T. J., and Rowan, N. J. 1973. "Evaluation of Breakaway Light Poles for Use in Highway Medians." *Highway Research Record* 460:123-136.
- Zegeer, C. V., and Cynecki, M. J. 1986 (December). "Selection of Cost-Effective Countermeasures for Utility Pole Accidents—User's Manual." Federal Highway Administration Report FHWA FHWA-IP-86-9. Washington, DC: U.S. Department of Transportation.

## APPENDIX

In this appendix, using standard structural theory (AASHTO 1985), sample calculations determined the average stresses in four couplings anchored to the base of a 40 ft light pole subjected to a wind speed of 90 mph. The derived wind pressure used an average diameter of 8 in., an average drag coefficient of 0.45, and a height coefficient of 1.1 for the 40 ft pole height. Stress concentration factors used were experimentally determined as described in this report. Mast, signal and luminaire arms are not considered in this calculation.

The user should also consider the use of the segmental method previously described in this report, particularly if signs are attached to the pole, or sharp changes in section are present along its length.

$$P = 0.00256 (V^2) \times C_d \times C_h \quad (1)$$

where: P = pressure against tube (lb/ft<sup>2</sup>)

V = wind velocity (mph)

C<sub>d</sub> = drag coefficient = 0.45

C<sub>h</sub> = height coefficient = 1.1

$$\text{When } V = 90 \text{ mph, } P = 0.00256 \times 0.45 \times 1.1 \times 90.00^2 = 10.26 \text{ lb/ft}^2$$

$$S = 8/12 \times H = 26.60 \text{ ft}^2 \quad (2)$$

where: S = exposed projected area (ft<sup>2</sup>)

H = height (ft) = 40.00 ft

D = diameter (in) = 10.00 in

$$M = P \times H \times S / 2 \quad (3)$$

where: M = moment (ft-lb)

$$M = 10.26 \times 40 \times 26.6 / 2 = 5,460.6 \text{ ft-lb} = 65,530 \text{ in-lb}$$

$$I_H = 0.3038 \text{ in}^4 \quad (4)$$

where: I<sub>H</sub> = Moment of inertia of hexagonal section (in<sup>4</sup>)

$$A_H = 1.9485 \text{ in}^2 \quad (5)$$

where: A<sub>H</sub> = Area of hexagonal section (in<sup>2</sup>)

$$I_N = \pi/64*(D_o^4 - D_i^4) = 0.0911 \text{ in}^4 \quad (6)$$

where:  $I$  = Moment of Inertia of notched section ( $\text{in}^4$ )

$D_o$  = outer section diameter (in.) = 1.300

$D_i$  = inner section diameter (in.) = 1.000

$$I_N = \pi/64*(1.300^4 - 1.000^4) = 0.0911 \text{ in}^4$$

$$A_N = \pi*(D_o^2 - D_i^2) \quad (7)$$

where:  $A_N$  = Area of notched section ( $\text{in}^2$ )

$$A_N = \pi*(1.300^2 - 1.000^2) = 0.5419 \text{ in}^2$$

$$I_{NS} = (I_N + A_N*D_s^2)*X_s \quad (8)$$

where:  $I_{NS}$  = Moment of inertia of notched sections in square configuration ( $\text{in}^4$ )

$D_s$  = Distance from centroid of arrangement to centroid of coupling (in.) = 5.30 in

$X_s$  = Number of couplings in square arrangement = 4

$$I_{NS} = (0.0911 + 0.5419*5.30^2)*4 = 61.26 \text{ in}^4$$

$$I_{ND} = (I_N + A_N*D_D^2)*X_{D1} + I_N*X_{D2} \quad (9)$$

where:  $I_{ND}$  = Moment of inertia of notched sections in diamond configuration ( $\text{in}^4$ )

$D_D$  = Distance from centroid of arrangement to centroid of coupling (in.) = 7.50 in

$X_{D1}$  = number of couplings at far points in diamond configuration = 2

$X_{D2}$  = number of couplings at centroid of diamond configuration = 2

$$I_{ND} = (0.0911 + 0.5419*7.5^2)*2 + 0.0911*2 = 61.33 \text{ in}^4$$

$$I_{HS} = (I_H + A_H*D_D^2)*X_s \quad (10)$$

where:  $I_{HS}$  = Moment of inertia of hexagonal section in square configuration ( $\text{in}^4$ )

$$I_{HS} = (0.3038 + 1.949*5.3^2)*4 = 220.2 \text{ in}^4$$

$$I_{HD} = (I_H + A_H*D_D^2)*X_{D1} + I_H*X_{D2} \quad (11)$$

where:  $I_{HD}$  = Moment of inertia of hexagonal section in diamond configuration ( $\text{in}^4$ )

$$I_{HD} = (0.3038 + 1.949*7.5^2)*2 + 0.30*2 = 220.4 \text{ in}^4$$

$$\sigma_{\text{NomS}} = M \cdot D_S / (I_{\text{NS}} \cdot X_{S2}) \quad (12)$$

where:  $\sigma_{\text{HS}}$  = Hexagonal section stress for V = 90 mph in square configuration (psi)

$X_{S2}$  = Number of couplings taking force at extreme = 2

$$\sigma_{\text{HS}} = 65530 \cdot 5.3 / 220.2 / 2 = 788.8 \text{ psi}$$

$$\sigma_{\text{NS}} = \sigma_{\text{HS}} \cdot K_t \quad (13)$$

where:  $\sigma_{\text{NS}}$  = Notched section stress for V = 90 mph in square configuration (psi)

$K_t$  = Stress concentration factor

$$\sigma_{\text{NS}} = 788.8 \cdot 7.15 = 5,640 \text{ psi (bending)}$$

$$\sigma_{\text{NS}} = 788.8 \cdot 10.8 = 8,519 \text{ psi (tension)}$$

$$\sigma_{\text{HD}} = M \cdot D_D / (I_{\text{ND}} \cdot X_{D3}) \quad (14)$$

where:  $\sigma_{\text{HD}}$  = Hexagonal section stress for V = 90 mph in diamond configuration (psi)

$$\sigma_{\text{HD}} = 65,530 \cdot 7.5 / 220.4 = 2,229.62 \text{ psi}$$

$$\sigma_{\text{ND}} = \sigma_{\text{HD}} \cdot K_t \quad (15)$$

where:  $\sigma_{\text{ND}}$  = Notched section stress for V = 90 mph in diamond configuration (psi)

$$\sigma_{\text{ND}} = 2,229.62 \cdot 7.15 = 15,940 \text{ psi (bending)}$$

$$\sigma_{\text{ND}} = 2,229.62 \cdot 10.8 = 24,080 \text{ psi (tension)}$$

$$\Delta S = (F / A_H \cdot K_t) \cdot 2 \quad (16)$$

where: F = Applied force (kip)

$$\Delta S = (4.25 / 1.9485 \cdot 7.15) \cdot 2 = 31.19 \text{ ksi (bending)}$$

$$\Delta S = (4.25 / 1.9485 \cdot 10.8) \cdot 2 = 47.11 \text{ ksi (tension)}$$

